

EVOLUTIONARY MODELS OF RED SUPERGIANTS: EVIDENCE FOR A METALLICITY-DEPENDENT MIXING LENGTH AND IMPLICATIONS FOR TYPE IIP SUPERNOVA PROGENITORS

SANG-HYUN CHUN,¹ SUNG-CHUL YOON,^{1,2} MOO-KEON JUNG,³ DONG UK KIM,⁴ AND JIHOON KIM¹

¹*Department of Physics and Astronomy, Seoul National University, 08826, Seoul, South Korea*

²*Monash Centre for Astrophysics, School of Physics and Astronomy, Monash University, Victoria 3800, Australia*

³*Department of Physics, Sogang University, 04107, Seoul, South Korea*

⁴*Department of Physics, Korea Advanced Institute of Science and Technology, 34141, Daejeon, South Korea*

(Received; Revised; Accepted)

ABSTRACT

Recent studies on the temperatures of red supergiants (RSGs) in the local universe provide us with an excellent observational constraint on RSG models. We calibrate the mixing length parameter by comparing model predictions with the empirical RSG temperatures in Small and Large Magellanic Clouds, Milky Way, and M31, which are inferred from the TiO band and the spectral energy distribution (SED). Although our RSG models are computed with the MESA code, our result may be applied to other stellar evolution codes, including the BEC and TWIN codes. We find evidence that the mixing length increases with increasing metallicity for both cases where the TiO and SED temperatures of RSGs are used for the calibration. Together with the recent finding of a similar correlation in low-mass red giants by Tayar et al, this implies that the metallicity dependence of the mixing length is a universal feature in post-main sequence stars of both low and high masses. Our result implies that typical Type IIP supernova (SN IIP) progenitors with initial masses of $\sim 10 - 16 M_{\odot}$ have a radius range of $400R_{\odot} \lesssim R \lesssim 800R_{\odot}$ regardless of metallicity. As an auxiliary result of this study, we find that the hydrogen-rich envelope mass of SN IIP progenitors for a given initial mass is predicted to be largely independent of metallicity if the Ledoux criterion with slow semiconvection is adopted, while the Schwarzschild models predict systematically more massive hydrogen-rich envelopes for lower metallicity.

Keywords: stars:evolution — stars:massive — stars:supergiants — stars:fundamental parameters — supernova:general

1. INTRODUCTION

The evolution of massive stars in numerical simulations depends on many different physical parameters that are related to the efficiency of convective energy transport, convective overshoot, semi-convection, rotation, mass loss, binarity, and metallicity, among others (e.g., Maeder & Meynet 2000; Langer 2012; Smith 2014). Given this complexity, details of massive star evolution are still much debated. However, there is a solid consensus that massive stars of B and O types in the mass range of ~ 9 to $\sim 30 M_{\odot}$ become red supergiants (RSGs) during the post-main sequence phase. Most of them would also die as RSGs, unless they underwent binary interactions during the course of their evolution (e.g., Podsiadlowski et al. 1992; Eldridge et al. 2013; Yoon et al. 2017) and/or strong enhancement of mass loss during the final evolutionary stages (e.g., Yoon & Cantiello 2010; Georgy 2012; Meynet et al. 2015).

RSG temperatures are mainly determined by the well-defined Hayashi limit, which is a sensitive function of the efficiency of convective energy transport and opacity (Hayashi & Hoshi 1961). This means that RSG stars can be used as reference standards for the calibration of some uncertain physical parameters used in stellar evolution models. In particular, RSG temperatures can provide an excellent observational constraint on the efficiency of the convective energy transport in RSG envelopes, which is commonly parameterized by the so-called mixing length in stellar evolution models (e.g., Kippenhahn & Weigert 1990).

This approach has become promising over the past decade with observational studies on RSG temperatures in different environments. RSG temperatures have been typically inferred by the model fitting to the TiO absorption band in optical spectra (e.g., Levesque et al. 2005, 2006; Massey et al. 2009). The temperatures from this method show a correlation with metallicity: higher temperatures at lower metallicities, which is consistent with the prediction from current several evolutionary models. Recently, however, Davies et al. (2013) recalculated the surface temperatures of RSGs in the Magellanic Clouds using the spectral energy distributions (SEDs) of RSGs. They found that the temperatures inferred from the strengths of TiO lines are systematically lower than those inferred from the SEDs. Interestingly, no clear metallicity dependence of RSG temperatures is found with this new approach (Davies et al. 2015; Gazak et al. 2015; Patrick et al. 2015), in contrast to the conclusions of previous observational studies with the TiO band. This calls for us to systematically inves-

tigate the metallicity dependence of RSG properties (cf. Elias et al. 1985).

In the above-mentioned observational studies, RSG locations on the Hertzsprung-Russel (RS) diagram have been compared mostly with the Geneva group models (e.g., Ekström et al. 2012; Georgy et al. 2013). The Geneva group uses $\alpha = 1.6H_P$, where H_P is the local pressure scale height at the outer boundary of the convective core. Although their models match fairly well the observed positions of red giants and supergiants of the Milky Way in the HR diagram, this value was chosen based on the solar calibration. In this study we aim to calibrate the mixing-length parameter by comparing the most recent observations of RSGs with stellar evolution models at various metallicities.

We choose the MESA code for the model calculations (Paxton et al. 2011, 2013, 2015). MESA is an open source code and currently widely used for various studies on stellar physics and stellar populations. Our new grid of models presented in this study will serve as a useful reference for future studies on massive stars using MESA in the community. A few studies indicate that different stellar evolution codes lead to diverse RSG structures for a given initial condition (Martins & Palacios 2013; Jones et al. 2015). However, this is mainly because of different input physics and the Hayashi line that determines RSG temperatures does not appear to significantly depend on different numerical codes as long as the same set of stellar structure equations are employed, as discussed below (Section 3). Therefore, our calibration of the mixing length parameter for different metallicities would be of interests to the users of several other stellar evolution codes as well.

Using our new grid of models, we also investigate the structure of Type IIP supernova (SN IIP) progenitors. In particular, both theoretical models on SN light curves and recent early-time observations of SN IIP imply much smaller radii of RSGs than predicted by conventional stellar evolution models (e.g., Dessart et al. 2013; González-Gaitán et al. 2015). In this study we discuss if the observed RSG temperatures can be consistent with the radii of SN IIP progenitors inferred from SN studies.

This paper is organized as follows. In Section 2, we describe the numerical method and physical assumptions adopted for this study. In Section 3, we discuss code dependencies of RSG models and the effects of different physical parameters on the evolution of RSGs. In Section 4, we confront our RSG models with observations, and discuss the metallicity dependence of the convective mixing length. In Section 5 we discuss the implications

of our result for the final structure of RSGs as SN IIP progenitors. We conclude this work in Section 6.

2. NUMERICAL METHODS AND PHYSICAL ASSUMPTIONS

We calculate our models with the MESA code. We construct the evolutionary models with both the Schwarzschild and Ledoux criteria for convection. With the Ledoux criterion, we consider inefficient semiconvection with an efficiency parameter of $\alpha_{\text{SEM}} = 0.01$. Slow semiconvection is implied by numerical simulations (Zaussinger & Spruit 2013). Note also that extremely fast semiconvection leads to results comparable to those with the Schwarzschild criterion. Therefore our models can roughly provide the boundary conditions for inefficient and efficient chemical mixing in chemically stratified layers.

In the MESA version we use (MESA-8845), the convective region is determined by the sign change of the difference between the actual temperature gradient and the adiabatic temperature gradient (the Schwarzschild criterion) or between the actual temperature gradient and the adiabatic temperature gradient plus the chemical composition gradient (the Ledoux criterion; Paxton et al. 2011). Recently Gabriel et al. (2014) point out that such a simple approach may lead to a physically incorrect determination of the convective boundary, especially when the chemical composition is discontinuous across the boundary. Soon after the completion of the present study, a new version of the MESA code has been released where a numerical scheme to rectify this issue is introduced (Paxton et al. 2017). As discussed below in Section 3, however, this does not significantly affect RSG temperatures.

Convective overshooting is considered with a step function and applied only for the hydrogen burning core. We calculate model sequences with three different overshooting parameters: $f_{\text{ov}} = 0.05, 0.15, \text{ and } 0.30$, which are given in units of the local pressure scale height at the upper boundary of the convective core. Note that Martins & Palacios (2013) recently suggested using $f_{\text{ov}} = 0.1 - 0.2$ based on the distribution of the main sequence stars on the HR diagram. Rotation is not considered in this study. The hydrogen burning core tends to be bigger with rapid rotation (Maeder & Meynet 2000; Heger et al. 2000), and this effect of rotation on the convective core size can be roughly considered with different overshooting parameters we use here. Note also that not a small fraction of massive stars are slow rotators (e.g., Mokiem et al. 2006; Ramírez-Agudelo et al. 2013; Simón-Díaz & Herrero 2014), in which case the effect of rotation would not be important.

For the calibration of the mixing length parameter, we construct RSG models with four different values: $\alpha = 1.5, 2.0, 2.5 \text{ and } 3.0$, which are given in units of the local pressure scale height. As shown below, the predicted RSG temperatures with these values can fully cover the observed RSG temperature range.

We consider four different initial metallicities: $Z = 0.004, 0.007, 0.02, \text{ and } 0.04$ scaled with the chemical composition of Grevesse & Sauval (1998), which roughly represent the metallicities of Small Magellanic Cloud (SMC), Large Magellanic Cloud (LMC), our galaxy (Milky Way), and M31, respectively. Many recent stellar evolution models adopt $Z = 0.014$ with the chemical composition of Asplund et al. (2005) and Asplund et al. (2009) for the Milky Way metallicity instead of $Z = 0.02$ with the composition of Grevesse & Sauval, but the predicted RSG temperatures are not significantly affected by the choice between the two options (see Section 3 below). We use the Dutch scheme for stellar wind mass-loss rates: the mass-loss rate prescriptions by Vink et al. (2001) for hot stars ($T_{\text{eff}} > 12500 \text{ K}$) and by de Jager et al. (1988) for cool stars ($T_{\text{eff}} < 12500 \text{ K}$). We use the simple photosphere boundary condition, which means that the full set of the stellar structure equations are solved up to the outer boundary that is defined by an optical depth of $\tau = 2/3$. For other physical parameters including the opacity table, we employ the default options of the MESA code for massive stars (i.e., the options in the file 'inlist_massive_defaults'). For each set of physical parameters, we calculate RSG models for different initial masses in the range from $9M_{\odot}$ to $39M_{\odot}$ with a $2M_{\odot}$ increment. All the calculations are stopped when the central temperature reaches 10^9 K , from which the envelope structure does not change significantly until core collapse (e.g., Yoon et al. 2017), except for some 9 and 11 M_{\odot} models that are stopped at the end of core helium burning due to a convergence problem.

For the discussion of code dependencies of RSG models in the section 3, we also present several RSG models with the BEC and TWIN codes. The BEC code, which is also often referred to as the STERN code in the literature (Heger et al. 2000), has been widely used for the evolutionary models of massive stars, including the recent Bonn stellar evolution grids (Brott et al. 2011). Like in our MESA models, the convective overshooting is treated with a step function in the BEC code and the overshooting parameter f_{ov} has the same meaning in both cases. The TWIN code is developed by P. Eggleton and his collaborators (Eggleton 1971; Eggleton & Kiseleva-Eggleton 2002; Izzard & Glebbeek 2006), and the WTTS package by Izzard & Glebbeek (2006) has been used for calculating RSG models with

the TWIN code in this study. In the TWIN code, convective overshooting is considered by modifying the convection criterion with an overshooting parameter δ_{ov} as $\nabla_{\text{rad}} > \nabla_{\text{ad}} - \delta_{\text{ov}}$, where ∇_{rad} and ∇_{ad} are radiative and adiabatic temperature gradients with respect to pressure in a logarithmic scale, respectively. The physical parameters adopted in the BEC and TWIN codes are described where appropriate in the following section. Note also that in all of these codes (MESA, BEC, and TWIN), the optical depth at the outer boundary is set to be $2/3$.

3. EFFECTS OF PHYSICAL PARAMETERS AND CODE DEPENDENCIES

3.1. Effects of the convection criterion and overshooting

In Fig. 1, we present evolutionary tracks of $15 M_{\odot}$ stars on the HR diagram calculated with MESA, BEC, and TWIN codes using different convective overshooting parameters and convection criteria. It is shown that the evolutionary tracks are significantly affected by the adopted physical parameters. As already found by numerous studies (e.g., [Brott et al. 2011](#); [Martins & Palacios 2013](#)), furthermore, the stars have a larger hydrogen burning core with a larger overshooting parameter. The main sequence width is enlarged and stars become more luminous with a larger overshooting parameter accordingly. For a given overshooting parameter in our MESA model, the evolutionary tracks of the Schwarzschild and the Ledoux models are identical for most of the main sequence phase. This is because the convective core size continues to decrease on the main sequence, for which both the Schwarzschild and the Ledoux criteria give the same convective core size. (see the green and blue lines in upper panel of Figure 1). Readers are referred to [Martins & Palacios \(2013\)](#) for more detailed discussion on the effect of various physical parameters on massive star evolution, in particular on the main sequence.

However, once the star reaches the RSG phase, the temperatures obtained with different overshooting parameters and different convection criteria converge to almost the same location on the HR diagram, for a given mixing length. Models with a larger overshooting parameter tend to have somewhat lower RSG temperatures as discussed in Section 4 in detail, but its effect is small compared to those of the mixing length and metallicity. It is shown that a larger mixing length leads to higher RSG temperatures, in good agreement with previous studies (e.g. [Schaller et al. 1992](#)).

As explained above in Section 2, a new scheme to determine the boundaries of convective zones has been introduced in the latest version of MESA ([Paxton et al.](#)

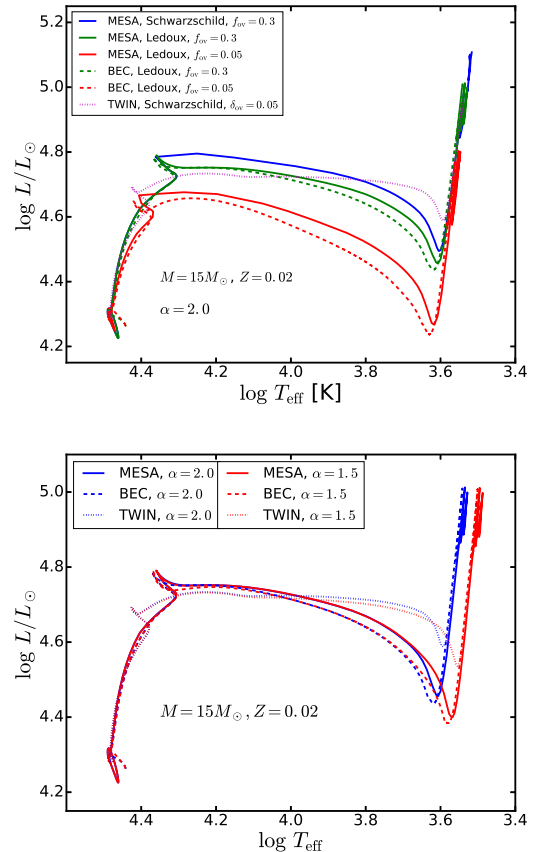


Figure 1. *Upper panel:* Comparison of the evolutionary tracks of $15 M_{\odot}$ stars at solar metallicity with a mixing length parameter of $\alpha = 2.0$ on the HR diagram for various overshooting parameters ($f_{\text{ov}} = 0.05$ and $f_{\text{ov}} = 0.3$ with the MESA and BEC codes, and $\delta_{\text{ov}} = 0.05$ with the TWIN code; see the text for the details) and convection criteria (Schwarzschild and Ledoux with a semiconvection parameter of $\alpha_{\text{SEM}} = 0.01$) calculated with the MESA (solid lines), BEC (dashed lines), and TWIN (dotted line) codes. *Lower panel:* Evolutionary tracks of $15 M_{\odot}$ stars at solar metallicity with mixing length parameters of $\alpha = 2.0$ (blue) and $\alpha = 1.5$ (red) obtained with the MESA (solid line), BEC (dashed line), and TWIN (dotted line) codes. The adopted overshooting parameters are $f_{\text{ov}} = 0.3$ for the MESA and BEC codes and $\delta = 0.05$ for the TWIN codes. The Ledoux criterion for convection with a semiconvection parameter of $\alpha_{\text{SEM}} = 0.01$ is adopted for the MESA and BEC models.

[2017](#)). We compare the results with and without this so-called predictive mixing scheme for a $15 M_{\odot}$ star at $Z = 0.02$ in Figure 2. We find that RSG temperatures are not significantly affected by this new scheme and the main conclusions of our work would not change either. However, we note that this new scheme can have important consequences in the inner structures if the Ledoux criterion is used, while models with the Schwarzschild criterion are hardly affected by this. In particular, the

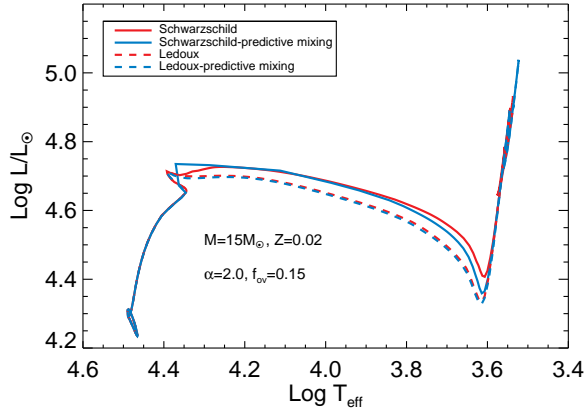


Figure 2. Evolutionary tracks of $15 M_{\odot}$ stars at $Z = 0.02$ with (blue) and without (red) the predictive mixing scheme. The adopted mixing length and the overshooting parameter are $\alpha = 2.0$ and $f_{\text{ov}} = 0.15$. The solid and dashed lines denote the Schwarzschild and the Ledoux models, respectively.

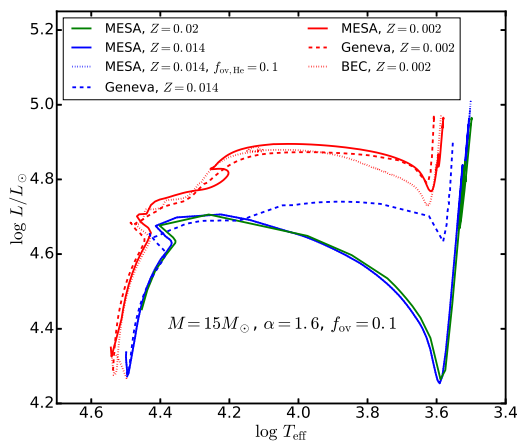


Figure 3. Evolutionary tracks of $15 M_{\odot}$ stars at $Z = 0.02$ with the chemical composition of Grevesse & Sauval (1998) (green), $Z = 0.014$ (blue) with the chemical composition of Asplund et al. (2009), and $Z = 0.002$ (red) with the mixing length parameter of $\alpha = 1.6$ and the overshooting parameter of $f_{\text{ov}} = 0.1$, calculated with the MESA (solid line), Geneva (dashed line), and BEC (dotted line) codes. The Schwarzschild criterion is used in all these calculations. The blue dotted line, which is overlapped with the blue solid line for the most part, is the $Z = 0.014$ MESA model where overshooting is also applied to the helium-burning core with $f_{\text{ov,He}} = 0.1$.

helium core splitting that has been commonly found in previous massive star models using the Ledoux criterion does not occur with the predictive mixing scheme. As a result, the size of the carbon core becomes much larger. For example, the helium (M_{HeC}) and carbon core (M_{CC}) masses in a $15 M_{\odot}$ star with the Ledoux

criterion at the pre-supernova stage are predicted to be $M_{\text{HeC}} = 5.0 M_{\odot}$ and $M_{\text{CC}} = 3.0 M_{\odot}$ when the predictive mixing scheme is used, compared to $M_{\text{HeC}} = 4.9 M_{\odot}$ and $M_{\text{CC}} = 1.9 M_{\odot}$ resulting from the previous method to determine the convective boundaries. A detailed investigation of this effect on the pre-supernova structure of massive stars would be an interesting subject of future studies.

3.2. Effects of metallicity and chemical composition

The metallicity effect is shown in Figure 3. As expected from the theory of the Hayashi limit (Hayashi & Hoshi 1961), lower metallicity (hence lower opacity) leads to higher RSG temperatures for a given α . This confirms the well known fact that the convective energy transport efficiency and the opacity are the primary factors that determines RSG temperatures.

In the present study we take the traditional value of $Z = 0.02$ with the chemical composition of Grevesse & Sauval (1998) as the metallicity of Milky Way. Many recent stellar evolution studies instead assume $Z = 0.014$ with the chemical composition given by Asplund et al. (2005) or Asplund et al. (2009). We also compare the two cases in Figure 3 but the difference in the RSG temperature is less than 50 K. We conclude that our results do not significantly depend on the choice between the two options for the Milky Way metallicity.

3.3. Code dependencies

We find some significant dependencies of the adopted numerical codes (cf., Martins & Palacios 2013; Jones et al. 2015). For example, the luminosity with the Ledoux criterion for a given overshooting parameter during the transition phase from the end of core hydrogen exhaustion until the beginning of the RSG phase is somewhat higher with MESA than with BEC (Figure 1). The reason for this discrepancy despite the same adopted convection parameters is very difficult to understand, and its clarification is beyond the scope of this paper. However, models from MESA, BEC and TWIN codes have very similar RSG temperatures. The difference in RSG temperatures along the Hayashi line resulting from different codes is smaller than ± 100 K for a given luminosity, as long as the same mixing length is adopted.

On the other hand, the models of the Geneva group, which have been most widely used in the literature for the comparison with observed RSGs, give significantly higher RSG temperatures on average, compared to those given by MESA, BEC and TWIN models. As an example, MESA and Geneva tracks for a $15 M_{\odot}$ star with $Z = 0.014$ and 0.002 are compared in Fig. 3, for which the same overshooting parameter ($f_{\text{ov}} = 0.1$) and

convection criterion (Schwarzschild) have been adopted. The Geneva group also considers overshooting above the helium-burning core, while it is applied only for the hydrogen-burning core in our MESA models. Therefore, in the figure, we also include an evolutionary track for which overshooting of $f_{\text{ov,He}} = 0.1$ is applied to the helium-burning core for comparison.

The Geneva group adopts the chemical composition of Asplund et al. (2005) except for ^{20}Ne for which they take the value of Cunha et al. (2006). Our MESA models with $Z = 0.014$ adopt the composition of Asplund et al. (2009), which is essentially the same with the Geneva model composition.

As shown in the figure, the difference in RSG temperatures along the Hayashi line between GENEVA and MESA models amounts to about 240 K, which is much bigger than the difference between MESA and BEC/TWIN models (< 100 K). The overshooting above the helium-burning core does not change the evolution on the HR diagram except that the luminosity during the last stage increases with the overshooting of the helium-burning core.

The reason that the Geneva group code gives distinctively different results compared to the other cases is difficult to understand. One possible reason would be the different numerical schemes adopted for the outermost layers of the star. With the default atmosphere boundary condition (i.e., the ‘simple photosphere’ option) in MESA, all the stellar structure equations are fully solved up to the outer boundary, which is also the case for the BEC and TWIN codes. The Geneva group solves the full set of stellar structure equations only for the inner layers, and treats the envelope and the atmosphere with a reduced set of equations (Meynet & Maeder 1997). In particular, the energy conservation equation is not considered in the envelope in the Geneva code. Although the luminosity due to the gravitational energy in the RSG envelope is negligibly small compared to the total luminosity, we still have to investigate how the omission of the energy equation can non-linearly influence the envelope structure. The treatment of the step overshooting in the Geneva code is also somewhat different from that of MESA: the Geneva code uses the adiabatic temperature gradient in the overshooting region instead of the radiative temperature gradient. However, this different prescription of overshooting is not likely to be responsible for such a big temperature difference of 200 K, given that the RSG temperatures from the TWIN code, which also adopts an overshooting scheme different from that of MESA and BEC as explained above, are very similar to the predictions of the MESA and BEC models.

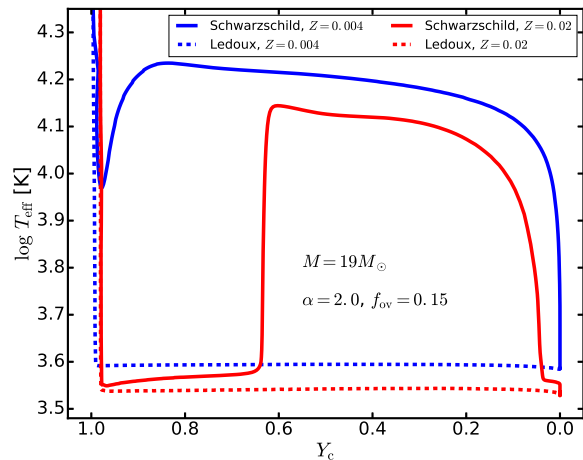


Figure 4. Evolution of the effective temperature of a $19 M_{\odot}$ star as a function of the helium mass fraction at the center during the post-main sequence phase, for the metallicities of $Z = 0.02$ (red) and $Z = 0.004$ (blue) and the Schwarzschild (solid line) and Ledoux criteria (dashed line) for convection. A semiconvection parameter of α_{SEM} is used for the Ledoux models.

We tentatively conclude that code dependencies of RSG temperatures along the Hayashi line are weak as long as the full set of stellar structure equations are solved up to the outer boundary of the star with a similar boundary condition. Our calibration of the mixing length with RSGs in this study can be relevant not only to MESA but also to several other stellar evolution codes including BEC and TWIN. A more detailed investigation of the effects of the numerical schemes on the Hayashi limit is needed for further clarification of this issue, which we leave as future work.

3.4. Additional remarks

It should also be noted that not all observed RSGs would be on the well defined Hayashi line. Some of them would be on the way to the Hayashi limit from the main sequence or the blue loop transition, and some others would be moving away from it due to the blue loop evolution or strong mass loss. Therefore, the observed distribution of RSG temperatures would depend not only on the Hayashi limit for a given mixing length and metallicity, but also on which fraction of the RSG lifetime is spent for the transition phases to/from the Hayashi limit.

The convection criterion becomes particularly relevant in this regard, because the post main sequence evolution can be significantly affected by its choice. As shown in Fig. 4 as an example, with the Ledoux criterion and slow semiconvection ($\alpha_{\text{SEM}} = 0.01$), a $19 M_{\odot}$ star with $\alpha = 2.0$ and $f_{\text{ov}} = 0.15$ becomes a RSG right after core hydrogen exhaustion, and spend the rest of its life as a

RSG until the end for both solar and SMC metallicities. With the Schwarzschild criterion, the stars of the same parameters undergo a blue loop at solar metallicity, and spend most of the post-main sequence phase as a blue supergiant (BSG) at SMC metallicity. RSG lifetimes of some selected models with two different convection criteria are presented in the Table 1. For SMC and LMC metallicities, RSG lifetimes become much shorter in the Schwarzschild case than in the Ledoux case with slow semiconvection. For the metal-rich cases ($Z \geq Z_{\odot}$), RSG lifetimes with the Schwarzschild criterion are comparable to those of the Ledoux models. In general, we find that the BSG to RSG lifetime ratio becomes higher with a higher mass, lower metallicity and smaller convective overshooting parameter, when the Schwarzschild criterion is adopted. This is in qualitative agreement with previous studies on massive stars. In particular, the number ratio of BSG to RSG stars has been predicted to increase with decreasing metallicity in the previous stellar evolution models with the Schwarzschild criterion (e.g., Langer & Maeder 1995; Eggenberger et al. 2002). In contrast, all our Ledoux models become RSGs shortly after core hydrogen exhaustion, and none of them undergoes a blue loop phase. As already discussed in previous studies (Eggenberger et al. 2002), none of the Schwarzschild and Ledoux models would be able to explain the observation that the BSG to RSG ratio increases with increasing metallicity. The reason for the difference between the Schwarzschild and Ledoux cases is difficult to understand and still a matter of great debate (e.g., Alongi et al. 1991; Stothers & Chin 1991; El Eid 1995; Langer & Maeder 1995; Bono et al. 2000). In the present study, we focus our discussion on RSG temperatures and leave the issue of BSG/RSG populations as a future work.

Finally, we would like to remind the readers of the fact that MESA adopts the so-called MLT++ treatment for the energy transport in radiation-dominated convective regions as a default option for massive stars (Paxton et al. 2013). This means that the superadiabaticity is reduced compared to the case of the standard mixing length theory. This makes the energy transport in the convective envelopes of RSGs that are close to the Eddington limit significantly more efficient than in the case of the standard mixing length approximation. RSG temperatures become higher with MLT++ accordingly when the luminosity is sufficiently high ($\log L/L_{\odot} \gtrsim 5.1$; see the related discussion in Section 4 below). The physics of the energy transport in radiation-dominated convective regions is poorly understood (see Paxton et al. 2013, for a detailed discussion on this issue). Note also that the convection in the

RSG envelope may become supersonic in the outermost layers, which may cause shock energy dissipation, where the simple approximation of the mixing length theory brakes down. Turbulence pressure might also play an important role. Therefore, these uncertainties should be taken into account as a caveat when we compare models with observations.

4. COMPARISON WITH OBSERVATIONAL DATA

In this section, we discuss the metallicity dependence of RSG temperatures using our MESA models compared to observed RSGs in SMC, LMC, our Galaxy and M31. For our discussion below, the RSG effective temperatures inferred from the strengths of the TiO band (e.g., Levesque et al. 2005, 2006; Massey et al. 2009; Gordon et al. 2016; Massey & Evans 2016) and the spectral energy distribution (SED; e.g., Davies et al. 2015; Gazak et al. 2015; Patrick et al. 2015) are referred to as TiO and SED temperatures, respectively. The bolometric luminosities of the RSGs with TiO temperatures were adopted from M_K rather than M_V in their catalogue (Levesque et al. 2005, 2006; Massey et al. 2009; Massey & Evans 2016), while the luminosity calibration relations of Davies et al. (2013) were used for the RSGs with SED temperatures.

For the mixing length calibration, we need to determine a representative RSG temperature at a given luminosity from our models. We find that most of the RSG models have a probability density function (PDF) of RSG temperatures with a well defined single peak. This means that the time-averaged RSG temperature ($\langle T_{\text{eff}} \rangle_{\text{RSG}} := \int_{t_{\text{RSG}}} T_{\text{eff}} dt / t_{\text{RSG}}$) agrees well with the mode value (T_{mode}) of the PDF of a given model sequence. Some exceptions are found for some Schwarzschild models that deviate from the Hayashi line for a certain fraction of the RSG phase. As an example, Figure 5 shows PDF of RSG temperatures for $15 M_{\odot}$ and $19 M_{\odot}$ models with $\alpha = 2.0$ and $f_{\text{ov}} = 0.15$. The PDFs were derived from the ratios of dt s of temperature bins to the RSG lifetime (t_{RSG}). To determine the RSG lifetime, we adopt $T_{\text{eff}} < 4800$ K ($\log T_{\text{eff}} = 3.68$) as the criterion for RSGs (i.e., $t_{\text{RSG}} = \int_{T_{\text{eff}} < 4800 \text{ K}} dt$), following Drout et al. (2009). It is found that the difference between $\langle T_{\text{eff}} \rangle_{\text{RSG}}$ and T_{mode} is less than about 0.03 dex for $15 M_{\odot}$ models for both the Schwarzschild and Ledoux cases. For $19 M_{\odot}$, the difference is as large as 0.1 dex with the Schwarzschild criterion, while it still remains small (< 0.03 dex) in the Ledoux case. Such a skewed temperature distribution as in the case of $19 M_{\odot}$ Schwarzschild models of the figure is found in particular for relatively low metallicity (SMC or LMC metallicity) and high initial mass ($M \gtrsim 19 M_{\odot}$) with the

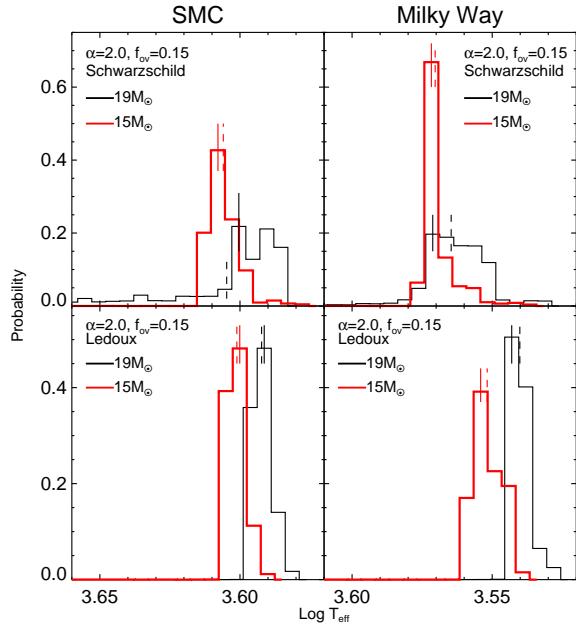


Figure 5. The probability density functions of RSG temperatures for 15 (red) and $19M_{\odot}$ (black) models with SMC and Milky Way metallicities in Schwarzschild and Ledoux convection criterion. The mixing length of $\alpha = 2.0$ and overshooting parameter of $f_{ov} = 0.15$ were adopted. The time-weighted temperatures of $\langle T_{eff} \rangle$ and mode temperatures of T_{mode} are indicated by vertical dashed line and solid line, respectively.

Schwarzschild criterion. In this case, the RSG temperature of a given model sequence would be better represented by $\langle T_{eff} \rangle$ than T_{mode} . We therefore decide to use the time-averaged temperature ($\langle T_{eff} \rangle_{RSG}$) and luminosity ($\langle L_{eff} \rangle_{RSG}$) for our mixing length calibration.

More specifically, using our model results, we interpolate $\langle T_{eff} \rangle_{RSG}$ and $\langle L \rangle_{RSG}$ at mixing length values from $\alpha = 1.5$ to 3.0 with 0.1 increment, for a given set of the convection criterion, f_{ov} , and metallicity. Then, we compare the temperatures of observed RSGs with those of interpolated values for a given luminosity. The deviation between the observations and the model temperatures is used to compute a χ^2 value. The mixing length value that gives the lowest χ^2 is determined to be our calibrated value that can best reproduce the observed RSG temperatures.

As discussed above, the effect of convective overshooting on RSG temperatures is minor compared to that of the mixing length. Following Martins & Palacios (2013), we take $f_{ov} = 0.15$ as the fiducial value in our discussion below.

4.1. Small Magellanic Cloud ($Z=0.004$)

We present the MESA evolutionary tracks with $f_{ov} = 0.15$ at SMC-like metallicity ($Z=0.004$) on the HR diagram compared with the observed SMC RSGs of Levesque et al. (2006) and Davies et al. (2015) in Figure 6. Although SED temperatures are known to be systematically higher than TiO temperatures (Davies et al. 2013), such an offset is not found with the SMC samples of the figure. The TiO temperatures given by Levesque et al. (2006) are more widely spread on the HR diagram than the SED temperatures of Davies et al. (2015). See Section 4.5 below for a related discussion.

We find that RSG models with the mixing length of $\alpha = 2.0$ and $\alpha = 2.5$ can roughly reproduce both the TiO and SED temperatures. RSG models with $\alpha = 1.5$ and 3.0 are too cool and too warm, respectively, compared to the observed RSGs. On the other hand, Patrick et al. (2015) found that RSG models of the Geneva group (Georgy et al. 2013) where $\alpha = 1.6$ are adopted are systematically warmer than the RSGs of Davies et al. (2015). This discrepancy between our models and Geneva models is because the Geneva code gives systematically higher RSG temperatures for a given mixing length than the MESA code does (see the discussion in Section 3) and because the models by Georgy et al. (2013) have a lower metallicity ($Z = 0.002$) than the value adopted in our models (i.e., $Z = 0.004$) that is typically invoked for the SMC.

In Figure 7, we present the time-weighted temperatures and luminosities of our RSG models on the HR diagram as well as best-fitted values to the observed RSG temperatures in the SMC. The observed RSGs are within the boundaries provided by the models with $\alpha = 1.5$ and $\alpha = 3.0$. In both the Schwarzschild and Ledoux cases, the effect of overshooting on RSG temperatures is minor compared to the effect of the mixing length. For a given mixing length, the time-weighted temperatures are slightly lower for the Ledoux models than for the Schwarzschild models. This is partly because of the fact that many of the Schwarzschild models at the SMC metallicity tend to deviate from the Hayashi line for a significant fraction of the RSG phase, while the Ledoux models remain on the Hayashi line for almost all of the RSG phase as explained in Sect. 3.

We find that with the Schwarzschild models and $f_{ov} = 0.15$, $\alpha = 2.0$ gives the best fits to the data for both TiO and SED temperatures. The corresponding values with the Ledoux models are $\alpha = 2.2$. These values become somewhat lower/higher for a smaller/larger overshooting parameter, as discussed in Sect. 4.5 below. We conclude that $\alpha \simeq 2.0$ can result in RSG models that can provide a reasonably good fit to RSG temperatures in the SMC.

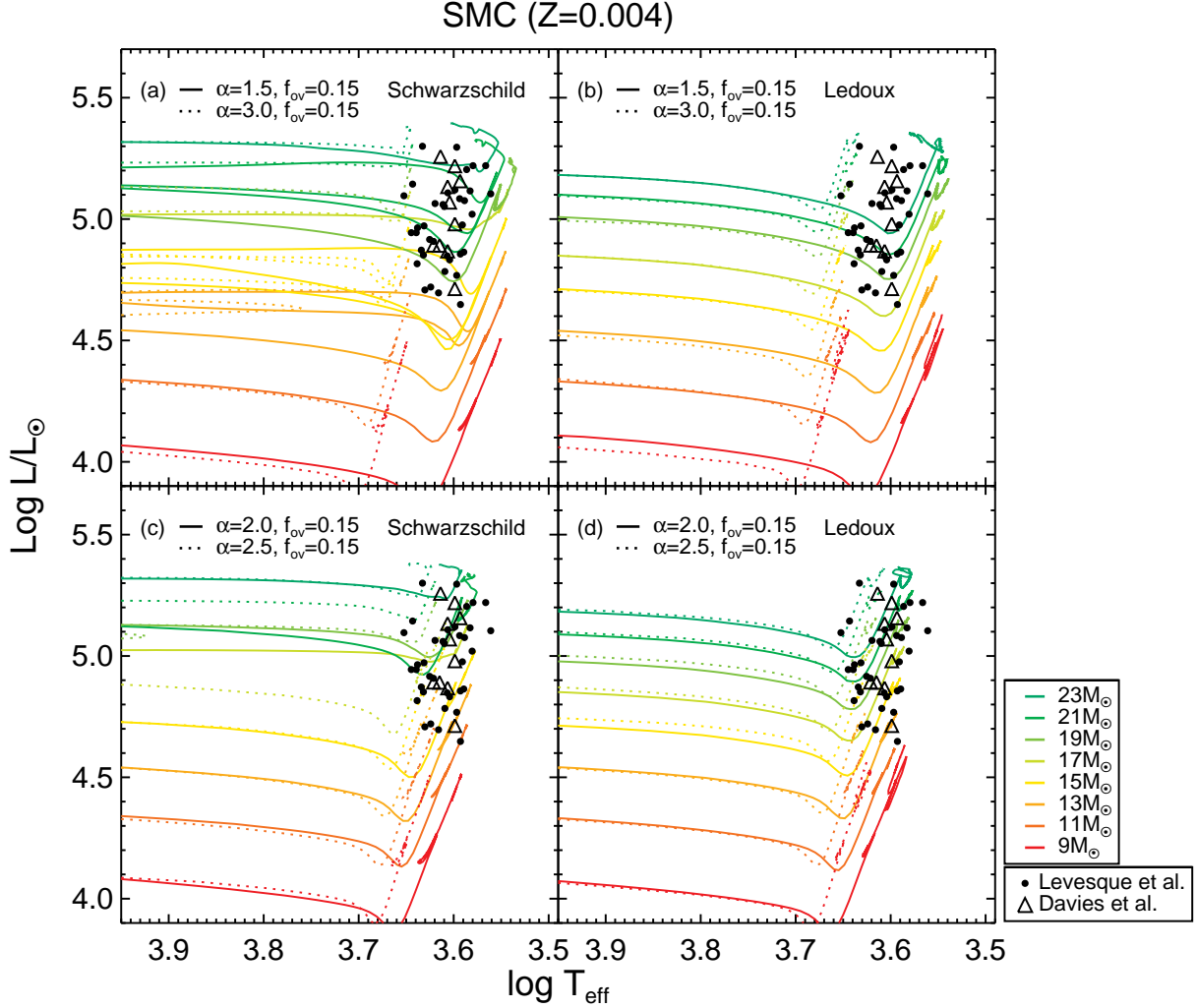


Figure 6. Evolutionary tracks on the HR diagram of the SMC-like metallicity ($Z = 0.004$) models with $f_{\text{ov}} = 0.15$. The Schwarzschild and Ledoux models are presented in the left and right panels, respectively. The tracks with $\alpha = 1.5$ (solid line) and $\alpha = 3.0$ (dotted line) are given in the upper panels, and those with $\alpha = 2.0$ (solid line) and $\alpha = 2.5$ (dotted line) in the lower panels. The initial mass of each track is indicated by the color of the line. The RSG samples of the SMC from Levesque et al. (2006, TiO temperatures) and from Davies et al. (2015, SED temperatures) are indicated by black dots and open triangles, respectively.

4.2. Large Magellanic Cloud ($Z=0.007$)

Figure 8 shows the MESA evolutionary tracks at the LMC-like metallicity ($Z=0.007$) and observed RSGs in the LMC from Levesque et al. (2006) and Davies et al. (2015). In contrast to the SMC case, the SED temperatures of Davies et al. (2013) are systematically higher than the TiO temperatures of Levesque et al. (2006) in the LMC, although there exists a significant overlap. We find that the RSGs models with $\alpha = 1.5$ and 3.0 have significantly lower and higher RSG temperatures compared to the observations, respectively. Models with $\alpha = 2.0$ and 2.5 (dotted lines) can roughly reproduce both the TiO and SED temperatures, as in the case of the SMC.

In Figure 9, we present the time-weighted temperatures and luminosities of our model grids at LMC-like metallicity on the HR diagram, compared with the observed RSGs. We find that the best fit values of α for the TiO temperatures are smaller than those for the SED temperatures: with $f_{\text{ov}} = 0.15$, $\alpha = 1.8$ (TiO) and 2.1 (SED) for the Schwarzschild models and $\alpha = 2.0$ (TiO) and 2.3 (SED) for the Ledoux models, respectively. This confirms the systematic offset between TiO and SED temperatures discussed by Davies et al. (2013).

4.3. Milky Way ($Z=0.02$)

In Figure 10, we compare the MESA evolutionary tracks with $f_{\text{ov}} = 0.15$ at solar metallicity ($Z=0.02$) and

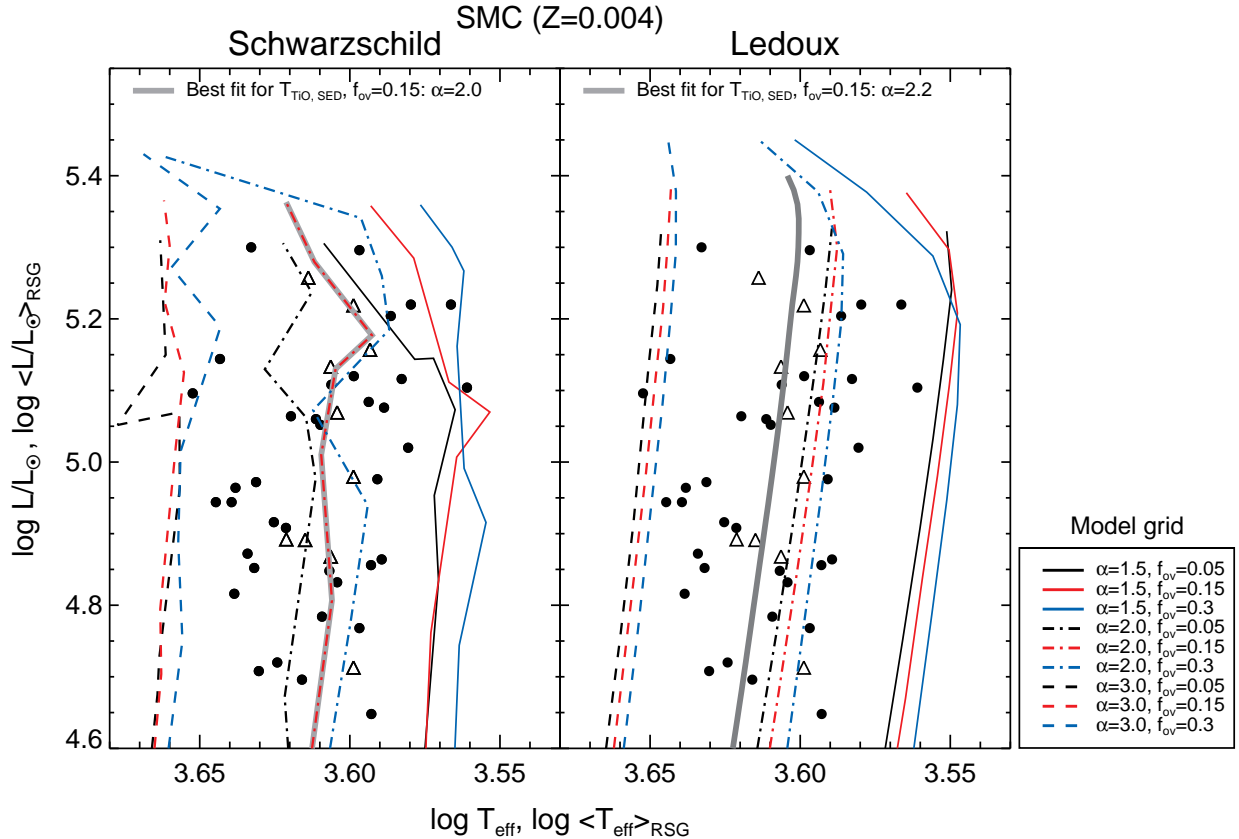


Figure 7. The time-weighted temperatures and luminosities (see Eqs. (1) and (2)) of the SMC-like metallicity ($Z = 0.004$) evolutionary tracks on the HR diagram, compared to the observed RSG samples of [Levesque et al. \(2006\)](#), TiO temperatures; filled circles) and [Davies et al. \(2015\)](#), SED temperatures; open triangles). The derived time-weighted values for three overshooting parameters ($f_{ov} = 0.05, 0.15$ and 0.3) are represented by black, red, and blue lines, respectively. The results for three mixing length parameters of $\alpha = 1.5, 2.0$ and 3.0 are indicated by solid, dot-dashed, and dashed lines, respectively. The best fits to TiO and SED temperatures, which are obtained with the models using $f_{ov} = 0.15$, are indicated by the thick grey lines. The corresponding calibrated mixing length values are $\alpha = 2.0$ and $\alpha = 2.2$ for the Schwarzschild and Ledoux cases, respectively. In the SMC, the best fit line is the same for both TiO and SED temperatures.

the observed Galactic RSGs of [Levesque et al. \(2005\)](#) and [Gazak et al. \(2014\)](#) on the HR diagram. As shown in Figure 10, the SED temperatures by [Gazak et al. \(2014\)](#) are significantly higher than TiO temperatures by [Levesque et al. \(2005\)](#) for the RSGs in the Milky Way. We find that the evolutionary tracks with $\alpha = 2.0$ and $\alpha = 2.5$ are roughly compatible with the positions of the observed RSGs from [Levesque et al. \(2005\)](#) and [Gazak et al. \(2014\)](#), respectively. The temperatures of the RSG models with $\alpha = 1.5$ are too low to reproduce the observed RSGs.

The time-weighted temperatures and luminosities of the RSGs models at solar-metallicity are shown in Figure 11. The lines with $\alpha = 2.0$ agree well with the TiO temperatures for both the Schwarzschild and Ledoux cases. The SED temperatures of [Gazak et al. \(2014\)](#) are in-between the lines of $\alpha = 2.0$ and 3.0 . For $f_{ov} = 0.15$, the best fits of the Schwarzschild models to the observations are found with $\alpha = 2.0$ and 2.6 for TiO and SED

temperatures, respectively. With the Ledoux models, $\alpha = 2.1$ and 2.8 give the best fits to the TiO and SED temperatures.

Note that the most luminous Galactic RSGs with $\log L/L_{\odot} \gtrsim 5.3$ are much cooler compared to our model predictions for all our considered mixing lengths and overshooting parameters. RSGs models tend to have lower temperatures for higher luminosities for $\log L/L_{\odot} \lesssim 5.3$, which roughly agrees with observations. However, the $\langle T_{\text{eff}} \rangle - \langle L \rangle$ lines begin to bend towards the left as the luminosity increases beyond $\log L/L_{\odot} \approx 5.3$. This is caused mainly by the MLT++ treatment of MESA that leads to more efficient energy transport compared to the case of the ordinary mixing-length formulation (see the discussion in Section 3). This makes very luminous RSGs quickly move away from the Hayashi line. For comparison, we present the model results for which the MLT++ option is turned off in Figure 11 (the third panel). The bending

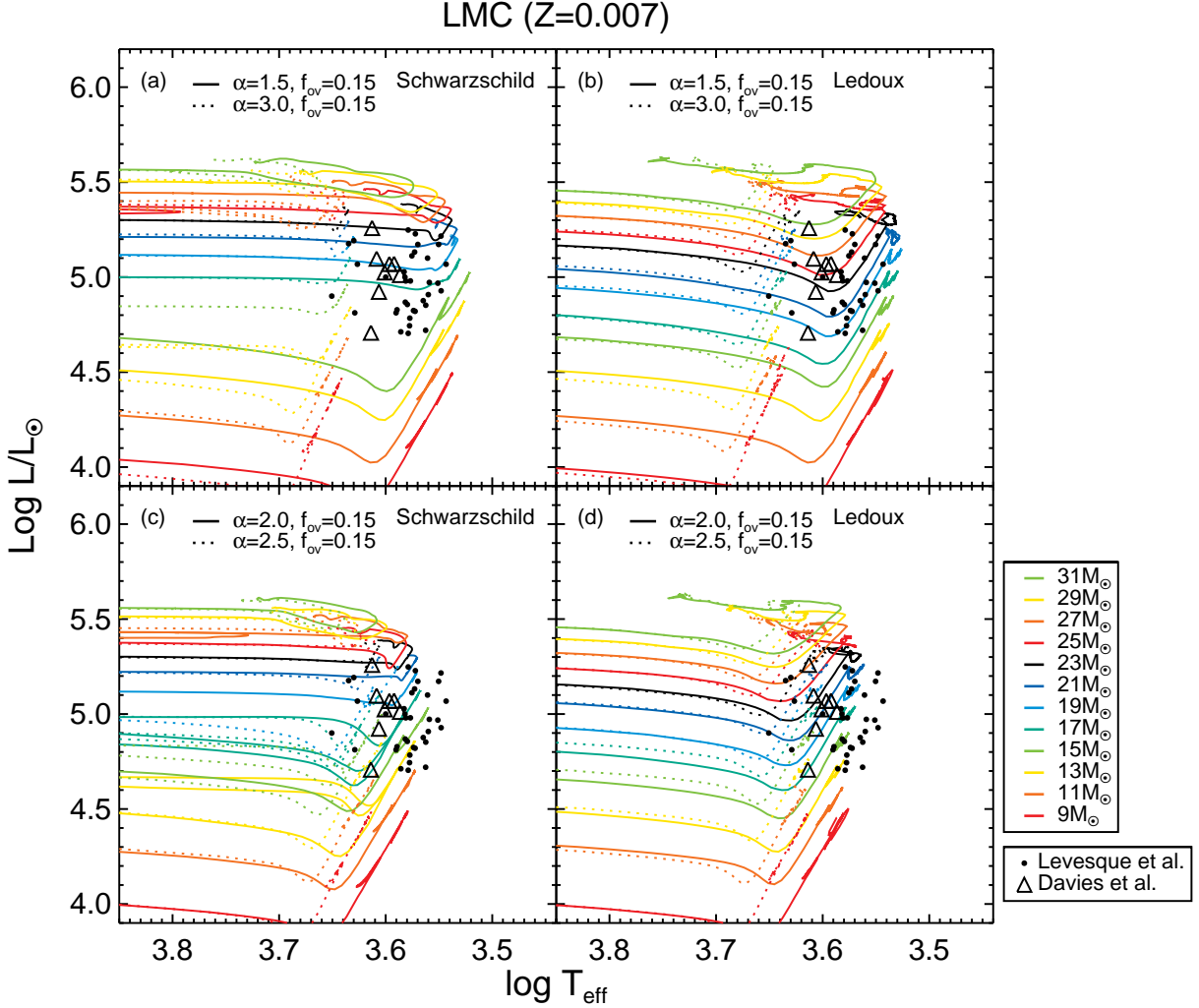


Figure 8. Same as in Figure 6, but for the LMC-like metallicity ($Z = 0.007$).

toward the left for $\text{log } L/L_{\odot} \gtrsim 5.3$ is still found because of strong mass loss from such luminous RSGs, but its degree is much weaker than in the case of MLT++. The temperatures of the most luminous RSGs are better matched by the models without MTL++, implying that the MLT++ treatment requires a caution when applied to the most luminous RSGs. To understand this discrepancy, we should address both the validity of the MLT++ treatment and the uncertainty in the temperature estimates of these most luminous RSGs that suffer strong reddening due to circumstellar dusts (e.g., Levesque et al. 2005; Gordon et al. 2016). The number of these luminous RSGs is small, and this bending with MLT++ does not affect our result of mixing length calibration.

4.4. M31 ($Z=0.04$)

In Figure 12, we show the M31-like metallicity ($Z = 0.04$) evolutionary tracks with $f_{\text{ov}} = 0.15$ on the HR

diagram, compared with the RSG sample of M31 provided by Massey & Evans (2016) who obtained the RSG temperatures using the TiO band. SED temperatures of RSGs in M31 are not available yet.

The most striking feature of the observed RSGs in M31 is the bifurcation in the temperature distribution: the warm sequence at around $\text{log } T_{\text{eff}} = 3.63$ and the cool sequence at $\text{log } T_{\text{eff}} = 3.57 - 3.61$. Massey & Evans (2016) investigated the lifetimes of RSG models at solar metallicity given by Ekström et al. (2012) as a function of the effective temperature. They found a lifetime gap for the temperature range of 4100 – 4150 K only for the $M = 25 M_{\odot}$ model sequence, and the bifurcation is not predicted by lower mass models. We could not find a lifetime gap at this temperature range with our models either. All of our RSG models at the M31 metallicity stay in the temperature range of 3900 – 4300 K only for a very short time (i.e., less than thousands of years), and spend the most of the RSG phase at lower temperatures.

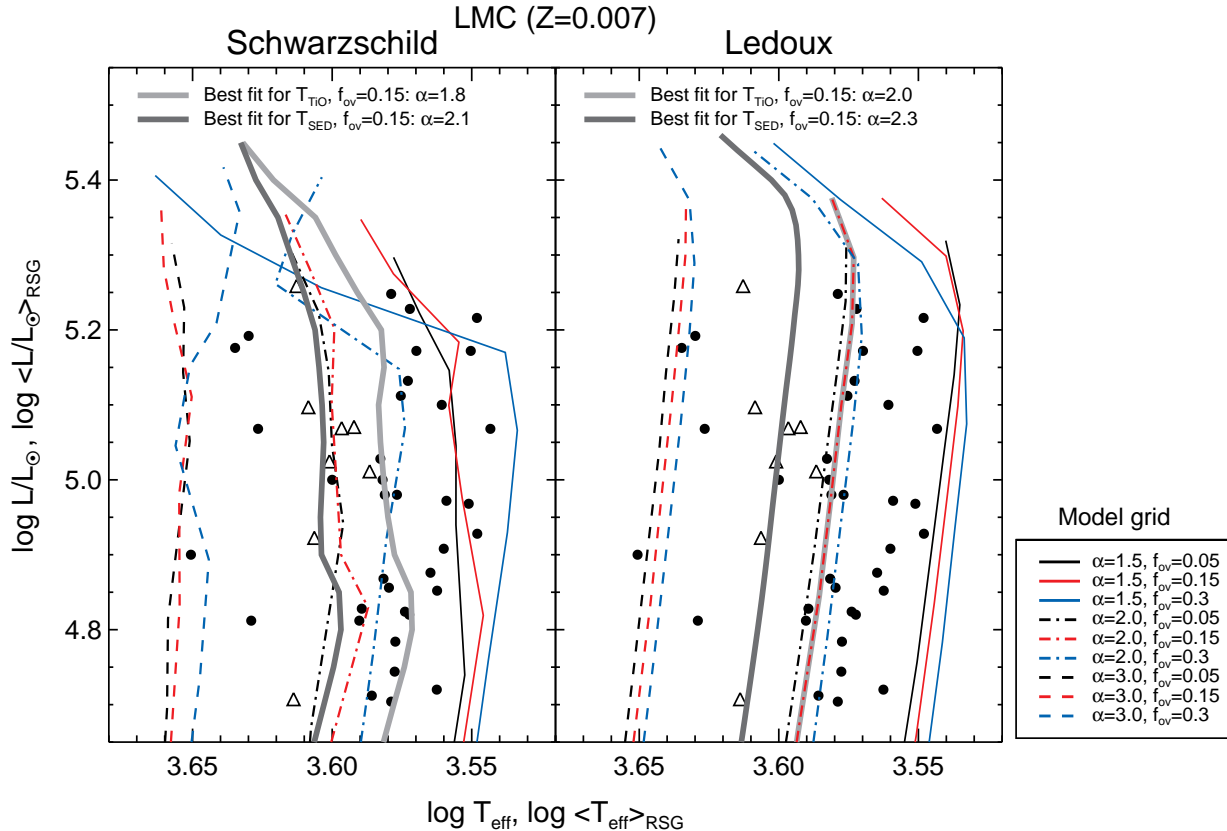


Figure 9. Same as in Fig. 7 but for the LMC-like metallicity ($Z = 0.007$). The best fit lines obtained from the models with $f_{ov} = 0.15$ for the TiO and SED temperatures are marked by the light and dark grey lines, respectively.

As shown in the figure, the RSG models with $\alpha = 2.0$ are too cool to explain the observations. The tracks with $\alpha = 2.5$ can roughly reproduce the location of the RSGs of the cool sequence. The RSGs of the warm sequence are too hot to be matched with our RSG models, even with the largest mixing length value (i.e., $\alpha = 3.0$).

In Figure 13, we present the time-weighted temperatures and luminosities of our evolutionary tracks at M31-metallicity, compared with observations. It is clearly seen that the RSG temperatures of the warm sequence cannot be explained with our considered range of mixing length values. We would need a significantly larger value of α than 3.0, or a lower metallicity to match the temperatures of the warm sequence. Given that the physical origin of this warm sequence is not clear and that our models do not predict the warm sequence, we calibrate α only with the RSGs of the cool sequence. We find that $\alpha = 2.7$ gives the best fits for both the Schwarzschild and Ledoux models. This is significantly larger than those found with the TiO data of the other galaxies.

As in the case of the Milky Way, the inclusion of MLT++ tends to make very luminous RSG models ($\log L/L_{\odot} \gtrsim 5.2$) warmer than those without MLT++ (compare the first and third panels of Figure 13) but

does not affect our mixing length calibration because of the small number of observed RSGs with $\log L/L_{\odot} > 5.2$.

4.5. Discussion

We have compared our evolutionary models with observed RSGs of several different metallicities and calibrated the mixing length for each metallicity. The result is summarized in Table 2 and Figure 14 where we present the calibrated mixing length values for three different overshooting parameters ($f_{ov} = 0.05, 0.15$ and 0.30), for both the TiO and SED temperatures. As shown above, the time-weighted temperatures are systematically lower for a larger f_{ov} and the resultant calibrated mixing length values are systematically larger for a larger f_{ov} . The mixing length values from SED temperatures are higher than those from TiO temperatures for LMC and Milky Way metallicities, as expected from the fact that SED temperatures are systematically higher than TiO temperatures. At SMC-like metallicity, the difference between the two cases is minor.

From both TiO and SED temperatures we find strong evidence that the mixing length depends on metallicity. With TiO temperatures, the metallicity dependence is particularly evident with the M31 sample of

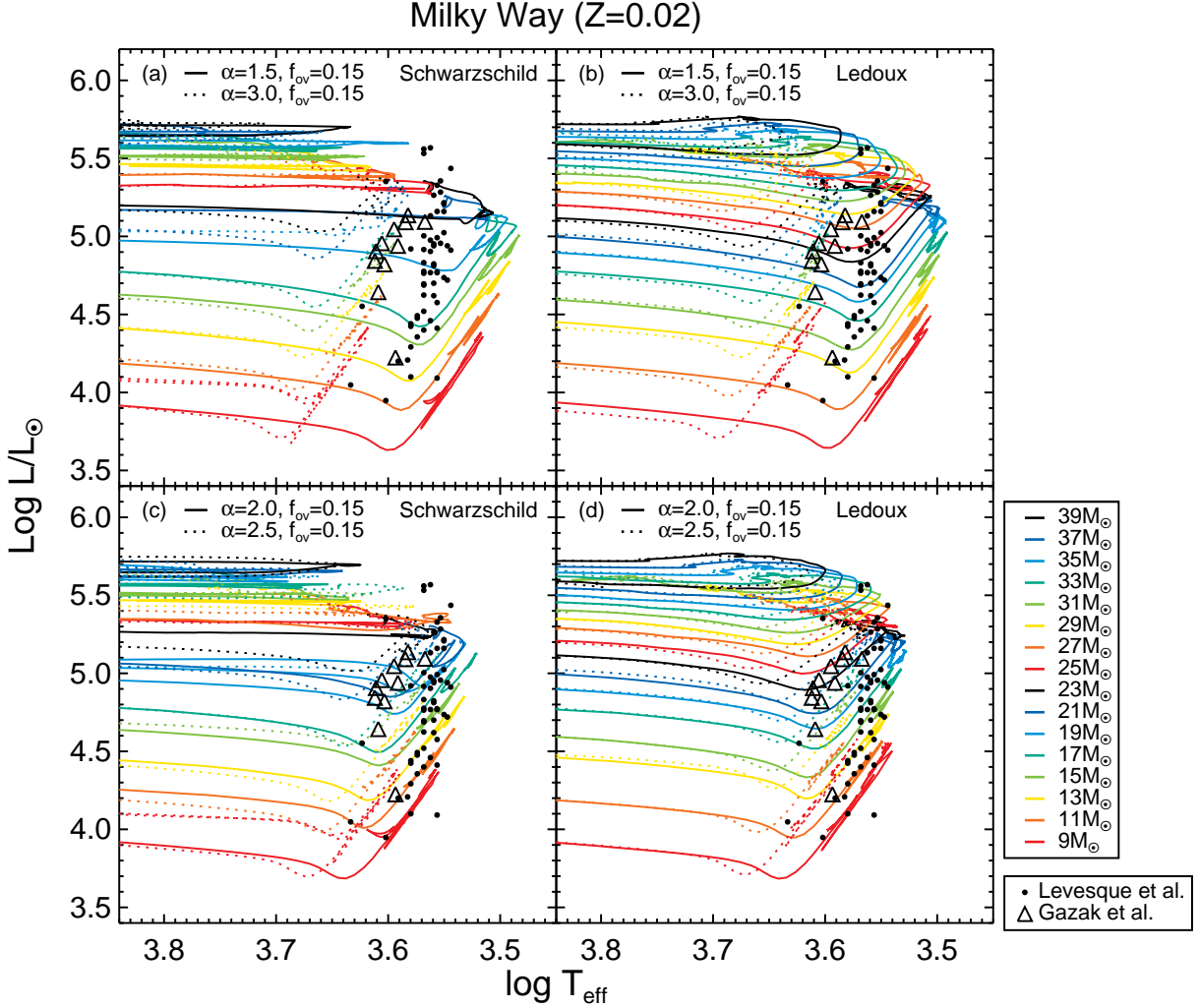


Figure 10. Same with Figure 6, but for solar metallicity ($Z = 0.02$). The compared Galactic RSG samples are taken from Levesque et al. (2005, TiO temperatures; filled circles) and Gazak et al. (2014, SED temperatures; open triangles).

Massey & Evans (2016). Interestingly, the TiO temperatures of the M31 RSGs of the cool sequence appears to be systematically higher than those of Galactic RSGs. Even if we use the $Z = 0.02$ models instead of $Z = 0.04$ models for the mixing length calibration of the M31 sample, we get $\alpha = 2.3$ and 2.4 for the Schwarzschild and Ledoux cases with $f_{\text{ov}} = 0.15$, respectively, which are significantly larger than the values of $\alpha = 2.0$ and 2.1 obtained with the TiO temperatures of the Galactic RSGs (Table 2). This cannot be easily explained without invoking a metallicity-dependent mixing length, given that the average metallicity of M31 RSGs is likely to be significantly higher than the Galactic value (see, however, Sanders et al. 2012).

The mixing length calibrated with TiO temperatures continuously decreases as the metallicity decreases from $Z = 0.04$ (M31) to $Z = 0.007$ (LMC), and suddenly increases at $Z = 0.004$ (SMC). This anomalous be-

havior at SMC-like metallicity is related to the wide spread of TiO temperatures of RSGs in SMC (Figure 7). Levesque et al. (2006) argued that this large spread results from enhanced effects of rotationally induced chemical mixing at relatively low metallicity of SMC. However, the temperature discrepancy during the RSG phase between non-rotating and rotating cases is not clearly seen in recently published stellar evolution models (Brott et al. 2011; Georgy et al. 2013). This scenario needs to be tested with a large grid of RSG models for a wide range of initial rotation velocities, which is beyond the scope of the present study.

The SED temperature ranges are much narrower than those of TiO temperatures (Figures 7, 9, and 11), given the small size of the selected RSG sample of Davies et al. (2015). In addition, the SED temperature range does not appear to depend on metallicity (Davies et al. 2015; Gazak et al. 2015; Patrick et al. 2015). As a result,

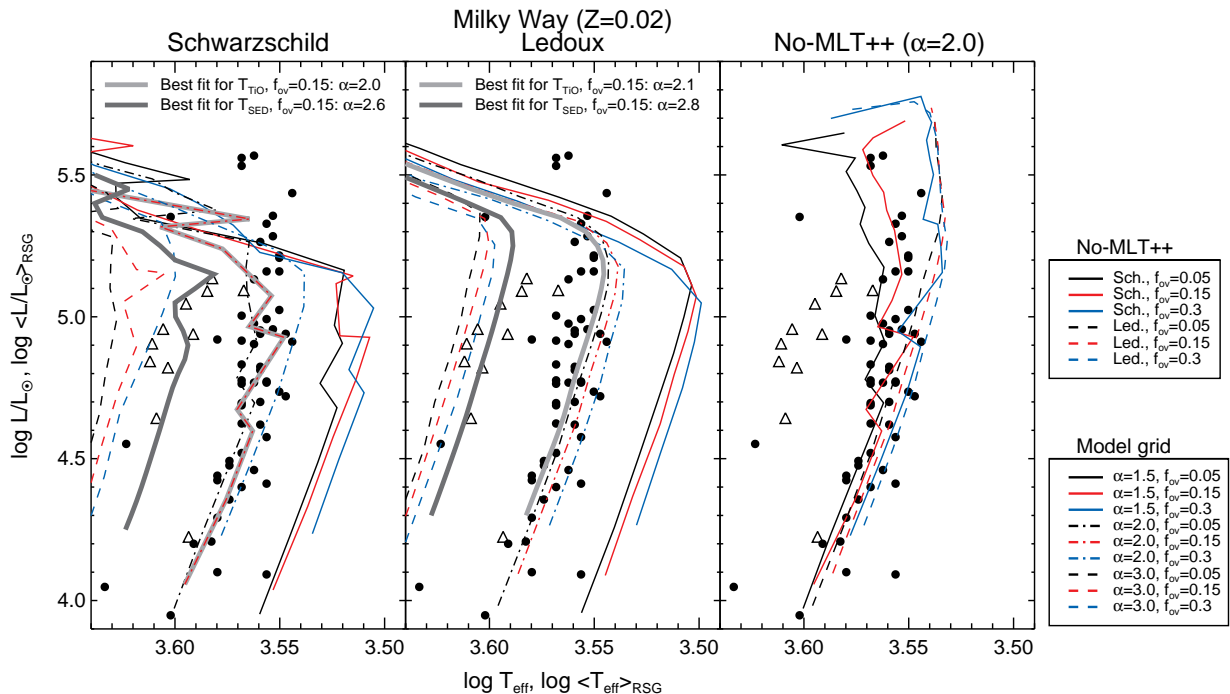


Figure 11. Same with Figure 7, but for solar metallicity ($Z = 0.02$). The results without the MLT++ treatment and with $\alpha = 2.0$ are also plotted in third panel for comparison. The compared Galactic RSG samples are taken from [Levesque et al. \(2005, TiO temperatures; filled circles\)](#) and [Gazak et al. \(2014, SED temperatures; open triangles\)](#).

the calibrated mixing length with SED temperatures is found to be a monotonically decreasing function of metallicity and its metallicity dependence appears to be stronger than in the case with TiO temperatures.

Interestingly, [Tayar et al. \(2017\)](#) has also found evidence for a metallicity-dependent mixing length in Galactic red giant stars, by analyzing the APOGEE-Kepler data. They calibrated the mixing length using low-mass star models ($0.6M_{\odot} - 2.6M_{\odot}$) for a metallicity range of $[Fe/H] = -2.0 \sim +0.6$, and concluded that the mixing length should be systematically smaller for lower metallicity (i.e., $\delta\alpha \approx 0.2$ per dex in metallicity) to match the temperatures of the observed red giant stars. Some evidence of the metallicity-dependent mixing length for red giants was also reported by [Chieffi et al. \(1995\)](#). These qualitatively conform to our finding with RSGs, and seems to indicate that less efficient convective energy transport at lower metallicity is a universal property of the convective envelopes of post-main sequence stars for both low and high masses.

This contradicts the theoretical result of [Magic et al. \(2015\)](#) who found that the mixing length increases with decreasing metallicity in three-dimensional numerical simulations¹. Note, however, that these simulations fo-

cused on stars with higher temperatures and gravities than those of RSGs and cannot be directly compared to our result. The mixing length theory has limitations to describe the RSG convection which can be supersonic in the outermost layers of the envelope. To our knowledge, there have been no theoretical studies using multi-dimensional numerical simulations done yet on the metallicity dependence of the convective energy transport in RSGs, and this should be an important subject of future studies.

It is also noteworthy that the discrepancy between the TiO and SED calibration values (i.e., $\Delta\alpha = \alpha_{\text{SED}} - \alpha_{\text{TiO}}$) is larger for higher metallicity. For example, with $f_{\text{ov}} = 0.15$ and the Ledoux criterion, we have $\Delta\alpha = 0.0, 0.3$, and 0.7 for SMC, LMC and Milky Way metallicities, respectively. This might imply that the layer suitable for the formation of the TiO band is located systematically farther above the continuum photosphere for higher metallicity (cf. [Chiavassa et al. 2011; Davies et al. 2013](#)). However, the size of the SED samples is much smaller than that of the TiO samples, and the selection bias might be an alternative reason for this tendency of increasing $\Delta\alpha$ with metallicity.

5. IMPLICATIONS FOR TYPE IIP SUPERNOVA PROGENITORS

Here we discuss the implications of our mixing-length calibration result for SN IIP supernova progenitors. For

¹ [Stothers & Chin \(1996\)](#) also previously suggested similar conclusions of [Magic et al. \(2015\)](#) based on the old observational data

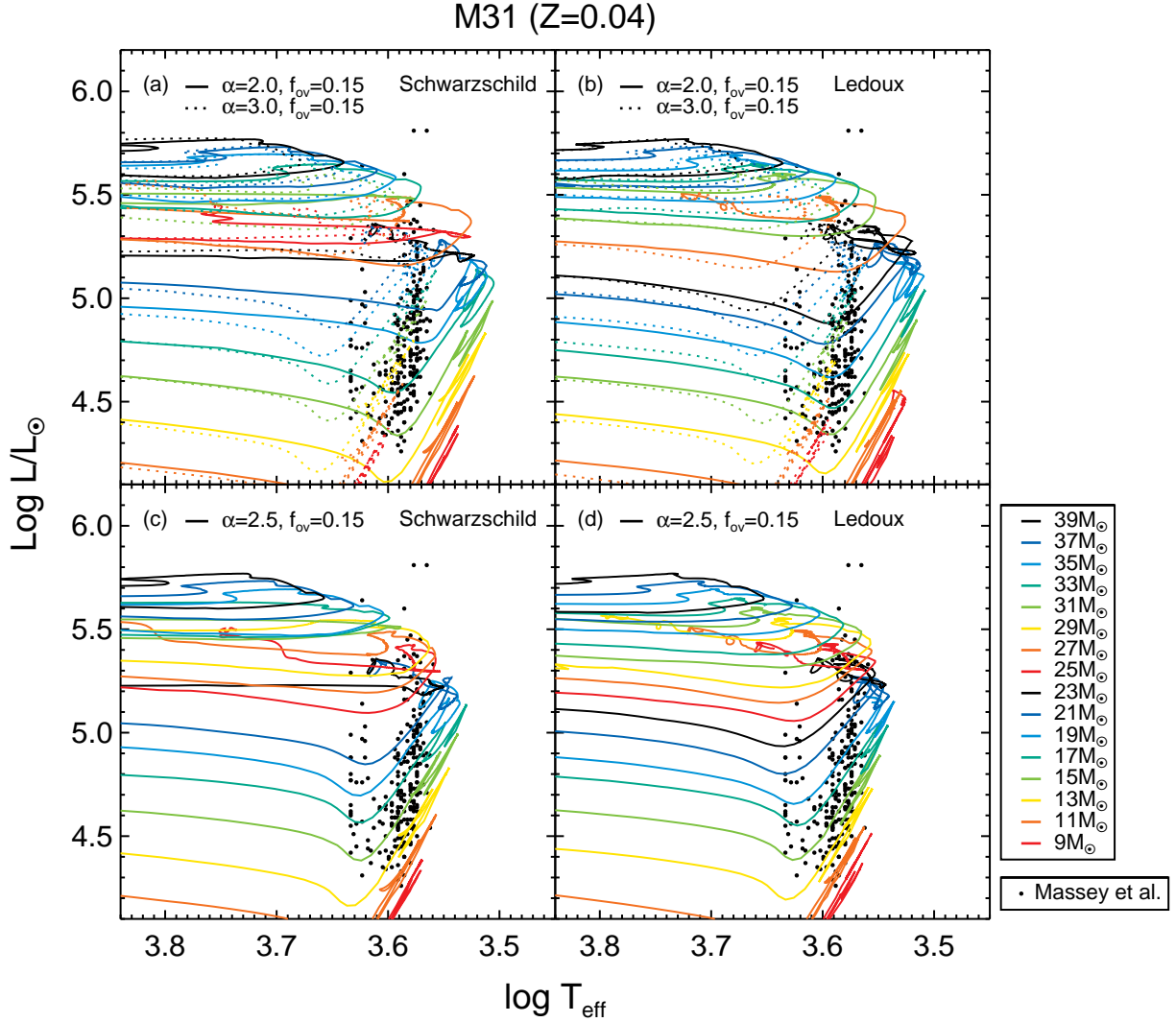


Figure 12. The M31-like metallicity ($Z=0.04$) evolutionary tracks on the HR diagram compared with the observed M31 RSG sample of Massey & Evans (2016). The tracks with $\alpha = 2.0$ (solid line) and $\alpha = 3.0$ (dotted line) are given in the upper panels, and those with $\alpha = 2.5$ (solid line) in the lower panels.

Table 2. Calibrated mixing length α

$f_{ov} =$	TiO						SED					
	Schwarzschild			Ledoux			Schwarzschild			Ledoux		
	0.05	0.15	0.30	0.05	0.15	0.30	0.05	0.15	0.30	0.05	0.15	0.30
SMC ($Z = 0.004$)	1.9	2.0	2.2	2.2	2.2	2.3	1.9	2.0	2.2	2.1	2.2	2.2
LMC ($Z = 0.007$)	1.8	1.8	2.0	1.9	2.0	2.0	2.0	2.1	2.3	2.3	2.3	2.4
MW ($Z = 0.02$)	2.0	2.0	2.2	2.1	2.1	2.2	2.5	2.6	2.8	2.7	2.8	2.9
M31 ($Z = 0.04$)	2.6	2.7	2.7	2.7	2.7	2.8	-	-	-	-	-	-
M31 ($Z = 0.02$) ^(a)	2.2	2.3	2.4	2.4	2.4	2.5	-	-	-	-	-	-

NOTE—(a) Solar metallicity models are used for the mixing length calibration with the M31 RSG sample.

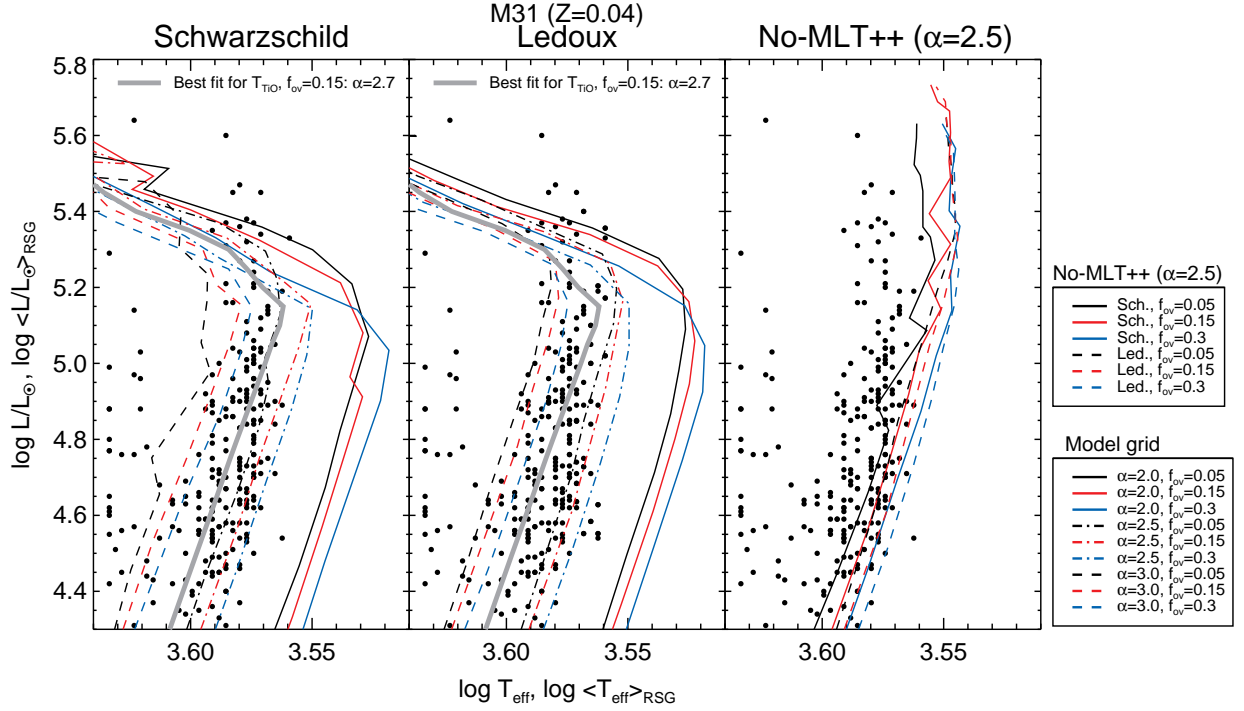


Figure 13. The time-weighted temperatures and luminosities of the M31-like metallicity ($Z=0.04$) evolutionary tracks of the Schwarzschild (the first panel) and Ledoux (the second panel) models. The M31 RSG sample of Massey & Evans (2016, TiO temperatures) are marked by filled circles. The results without the MLT++ treatment and with $\alpha = 2.5$ are presented in the third panel for comparison. The models of three overshooting parameters ($f_{\text{ov}} = 0.05, 0.15$ and 0.3) are represented by black, red, and blue lines, respectively. The results of three mixing length parameters of $\alpha = 2.0, 2.5$ and 3.0 are plotted by solid, dot-dashed, and dashed lines, respectively. The light grey lines in the first and second panels are the best fit lines obtained from the models with $f_{\text{ov}} = 0.15$.

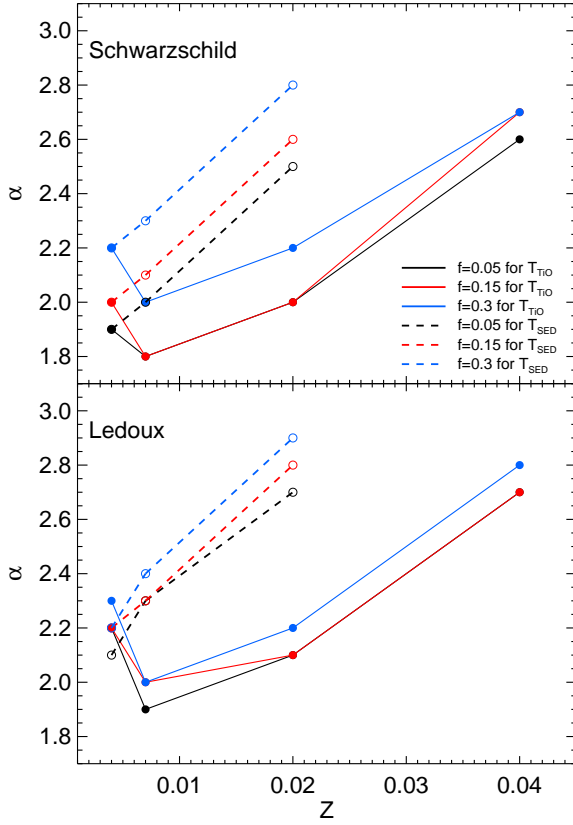


Figure 14. The calibrated mixing length values for TiO (solid lines) and SED (dashed lines) temperatures as a function of metallicity obtained with the Schwarzschild (upper panel) and Ledoux (lower panel) models. The adopted overshooting parameters in the models are indicated by three different colors: black ($f_{\text{ov}} = 0.05$), red ($f_{\text{ov}} = 0.15$), and blue ($f_{\text{ov}} = 0.30$).

this purpose, in the figures of Appendix A (Figures 16, 17, 18, and 19), we present the final radius, total mass M_{final} , and hydrogen envelope mass $M_{\text{H-env}}$ at the final evolutionary stage, which we obtain by interpolating the results of our last computed models for our calibrated mixing length parameters. Examples of physical structures of our last computed models are indicated in Table 1.

5.1. Final and hydrogen envelope masses

As shown in Figure 1, different choices of the mixing length within our considered parameter space can hardly alter the evolution on the main sequence. However, the role of the mixing length on the mass-loss history during the post main sequence evolution is significant because the mass-loss rate depends on the effective temperature of a star, as well as its luminosity. In our models, the mass-loss rate prescription for RSGs by de Jager et al. (1988) is adopted, which has the power-law relation of $\dot{M} \propto L^{1.769} T_{\text{eff}}^{-1.676}$. Given that RSG

models with $\alpha = 1.5$ and 3.0 have a temperature difference of about 0.1 dex on average (Figures 7, 9, and 11), a smaller mixing length parameter leads to more mass loss. For example, our Ledoux models at solar metallicity with $M_{\text{init}} = 25 M_{\odot}$ and $f_{\text{ov}} = 0.15$ have final masses of $14.1 M_{\odot}$ and $15.6 M_{\odot}$ for $\alpha = 1.5$ and 3.0, respectively. This leads to slightly different results on the initial-final mass relations obtained with the TiO and SED calibration results particularly at solar metallicity for which the difference between α_{TiO} and α_{SED} is significant.

The impact of the mixing length on the final mass is minor compared to that of the overshooting parameter. A larger f_{ov} leads to substantially higher luminosities for a given initial mass and the corresponding mass-loss rates are higher throughout the whole evolutionary stages. For example, the Ledoux models with $M_{\text{init}} = 25 M_{\odot}$ and $\alpha = 2.0$ at solar metallicity have final masses of 16.1 and 12.9 for $f_{\text{ov}} = 0.05$ and 0.30, respectively. The relations of the initial mass - the final helium core and hydrogen envelope masses are also significantly affected by the overshooting accordingly. A larger f_{ov} results in a smaller final mass, a larger helium core mass, and a smaller hydrogen-envelope mass.

Note that the metallicity dependence of the final mass for a given initial set of physical parameters appears stronger in the Schwarzschild models than in the Ledoux models. In the Ledoux models the final mass for a given initial mass does not change significantly with metallicity, while in the Schwarzschild models the final mass becomes much higher for a lower metallicity. For example, with the Schwarzschild criterion and $f_{\text{ov}} = 0.15$, a star with $M_{\text{init}} = 35 M_{\odot}$ is predicted to have $M_{\text{final}} \approx 30 M_{\odot}$ at SMC metallicity and $M_{\text{final}} \approx 18 M_{\odot}$ at solar metallicity. With the Ledoux criterion, the corresponding final masses are $M_{\text{final}} \approx 18 M_{\odot}$ and $16 M_{\odot}$, respectively (see Figures 16 and 18). This can be explained as the following. In the Dutch scheme for mass loss of the MESA code, the mass-loss rate prescription for RSG stars by de Jager et al. (1988) does not consider a metallicity dependence, while the mass-loss rate for hot stars is given by a function of metallicity (i.e., $\dot{M} \propto Z^{0.85}$) as suggested by Vink et al. (2001). With the Ledoux criterion, stars quickly crosses the Hertzsprung gap once hydrogen is exhausted in the core and spend the rest of the lifetime on the Hayashi line as RSGs for the metallicities considered in our study (Figure 4). Given that mass-loss is usually more important during the RSG phase than on the main sequence, the final masses of the Ledoux models do not sensitively depend on the metallicity. With the Schwarzschild criterion, metal-rich models ($Z \geq Z_{\odot}$) generally behave like the Ledoux models although the

blue loop is found for some initial masses. However, at sub-solar metallicity, the Schwarzschild models tend to spend most of the post-main sequence lifetime as a BSG as shown in Figure 4. The mass-loss rates of such BSGs with $T_{\text{eff}} < 20000$ K are higher than those of the corresponding main sequence stars (Vink et al. 2001), and can play a major role for the final mass if a star spends most of the post-main sequence phase as a BSG. However, the BSG mass-loss rates are much lower than those of RSGs for a given luminosity and decrease with decreasing metallicity, according to the prescription of Vink et al. (2001). This can explain the reason why the Schwarzschild models of SMC and LMC metallicities have much higher final masses than the corresponding Ledoux models. These different predictions of the Schwarzschild and Ledoux models can be tested with observations, in principle, in particular by looking at the BSG/RSG number ratio as a function of metallicity as mentioned in Section 3 above.

It is also important to note that all of our Ledoux models have $M_{\text{H-env}} < 10 M_{\odot}$ regardless of metallicity, while the Schwarzschild models at sub-solar metallicities can have $10 M_{\odot} < M_{\text{H-env}} < 20 M_{\odot}$ for $M_{\text{init}} \gtrsim 15 M_{\odot}$. Given that the hydrogen envelope mass is strongly correlated with the plateau duration and luminosity of a SN IIP, this prediction can be tested if a good statistics of SNe IIP from metal poor environments can be provided in future SN surveys. For example, Utrobin & Chugai (2009) argues for a very massive hydrogen envelope mass ($M_{\text{H-env}} \approx 14 M_{\odot}$) in the SN IIP 2004et, which cannot be explained by our Ledoux models. However, one of the reasons for the relatively small hydrogen envelope masses with the Ledoux criterion is that the RSG mass-loss rates are not assumed to decrease with decreasing metallicity. No strong evidence for the metallicity dependence of the RSG wind mass-loss rate is found so far, which is still a matter of debate (see van Loon 2006, for a review). Another caveat here is that no SN IIP progenitors with $M_{\text{init}} \gtrsim 16 M_{\odot}$ have been robustly identified yet (Smartt 2009, 2015). This might imply that more massive stars are likely to collapse to a BH, in which case bright SNe IIP from massive progenitors with $M_{\text{H-env}} > 10 M_{\odot}$ would be rare even if the prediction of the Schwarzschild models was correct.

5.2. Radius

One of the best ways to infer the radii of SN IIP progenitors is to compare the theoretically predicted light curves and colors of SNe IIP with observations (e.g., Nakar & Sari 2010; Rabinak & Waxman 2011; Morozova et al. 2016; Shussman et al. 2016). Dessart et al. (2013), for example, concluded that su-

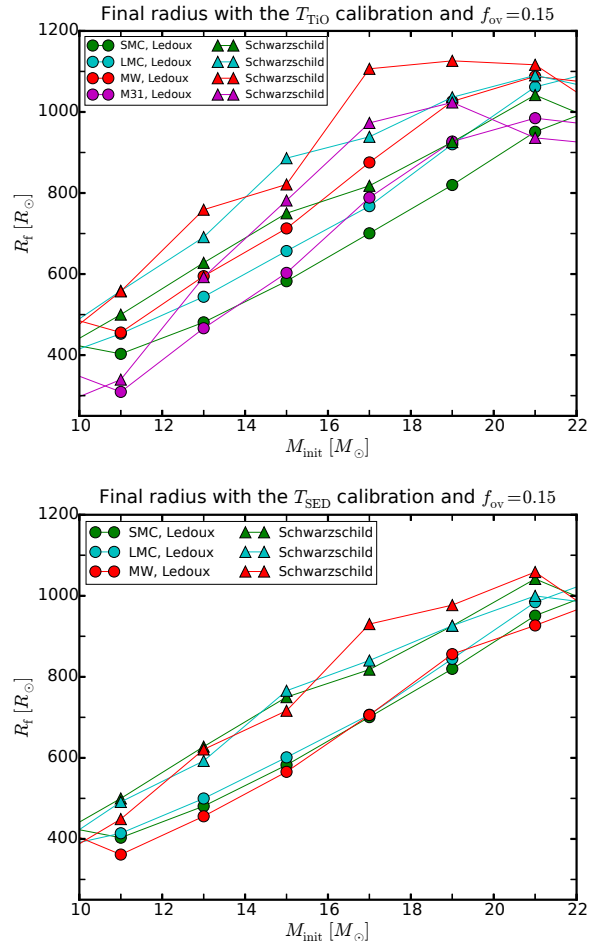


Figure 15. Predicted final radii of Type IIP progenitors with our calibrated mixing lengths and $f_{\text{ov}} = 0.15$. The TiO and SED calibration results are given in the upper and lower panels, respectively. The filled circles and triangles denote the predictions with the Schwarzschild and Ledoux models, respectively. The different metallicities are indicated by different colors: green ($Z = 0.004$; SMC), sky blue ($Z = 0.007$; LMC), red ($Z = 0.02$; Milky Way), and purple ($Z = 0.04$; M31).

pernova models with $R \lesssim 500 R_{\odot}$ can best explain the U-band evolution of typical SNe IIP and that a larger size leads to too blue colors compared to observations. González-Gaitán et al. (2015) measured the rise-times of light curves for a large sample of observed SNe IIP and found that the average rise time is 7.5 ± 0.3 d. By comparing this result with theoretical predictions, they concluded that $R \lesssim 400 R_{\odot}$ is necessary to explain this short rise-time. Shock breakout and early time observations of the SNe IIP KSN2011a and KSN2011d also imply relatively small radii of their progenitors (i.e., $\sim 280 R_{\odot}$ and $\sim 490 R_{\odot}$, respectively, Garnavich et al. 2016). Some other studies suggested that larger radii than $\sim 500 R_{\odot}$ can still be consis-

tent with observations (e.g., Utrobin & Chugai 2009; Valenti et al. 2014; Bose et al. 2015; Morozova et al. 2016). The caveat in these conclusions is that the early time evolution of SNe IIP can be strongly affected by the presence of dense circumstellar material (e.g., González-Gaitán et al. 2015; Garnavich et al. 2016; Morozova et al. 2017; Moriya et al. 2017; Dessart et al. 2017).

Our mixing length calibration allows us to predict SN IIP progenitor sizes that can be most consistent with the observed properties of RSGs. In Figure 15, we present the predicted final radii of SN IIP progenitors based on our TiO and SED calibration results, for the initial mass range of $11 - 21 M_{\odot}$ (see also Figures 16, 17, 18, and 19). Some of our models with $M_{\text{init}} = 9.0 M_{\odot}$ have been followed only up to the core helium exhaustion, and are not suitable for the prediction of the final stage. For $M_{\text{init}} > 21 M_{\odot}$, the effect of MLT++ that might lead to significant underestimates of RSG radii is too strong (see Section 4). Observations also imply that SNe IIP from such massive progenitors are rare. From the figure, we make the following remarks.

Firstly, there is no clear metallicity dependence of the progenitor radius. The TiO calibration gives a systematically larger radius for a given initial mass as the metallicity increases from $Z = 0.004$ (SMC) to $Z = 0.02$ (solar) but this trend is not extended to $Z = 0.04$ (M31) for which the predicted radii are smaller than those of the solar metallicity for a given convection criterion. Note also that the M31 models have even smaller radii than the SMC models for $M_{\text{init}} \lesssim 15 M_{\odot}$. With the SED calibration, the scatter due to metallicity is much smaller than in the TiO case. For the initial mass range of $10 \lesssim M_{\text{init}} \lesssim 16 M_{\odot}$ where the majority of SNe II are expected (Smartt 2009), the final radius ranges from $400 R_{\odot}$ to $600 R_{\odot}$ with the Ledoux criterion and from $400 R_{\odot}$ to $800 R_{\odot}$ with the Schwarzschild criterion, regardless of metallicity.

Secondly, the relatively small radii of $R \lesssim 500 R_{\odot}$ for SN IIP progenitors suggested by Dessart et al. (2013) and González-Gaitán et al. (2015) agree best with the predictions given by the Ledoux models with the SED calibration. However, the very small radius of $R \approx 280 R_{\odot}$ inferred for the progenitor of the SN IIP KSN2011a (Garnavich et al. 2016) is found only with $M_{\text{init}} \leq 11 M_{\odot}$ at M31 metallicity. In general, $R \gtrsim 400 R_{\odot}$ is predicted within our considered parameter space.

6. CONCLUSIONS

We have presented RGS models with the Schwarzschild and Ledoux criteria using the MESA code, and cal-

ibrated the mixing length parameter at SMC, LMC, Milky Way, and M31 metallicities by comparing the effective temperatures given by our RSG models with the empirical RSG temperatures inferred from the TiO band and SED (Section 4). We also discussed its implications for SN IIP progenitors (Section 5).

The main conclusion of this study is that the mixing length in RSGs depends on metallicity. For both cases of TiO and SED temperatures, we find that the mixing length is an increasing function of metallicity (Table 2 and Figure 14). Our finding probably indicates that the efficiency of the convective energy transport in RSGs becomes higher for higher metallicity. This result is in qualitatively accordance with the recent finding of the correlation between mixing length and metallicity in low-mass red giant stars by Tayar et al. (2017), implying that this correlation is a universal feature in post-main sequence stars for both low and high masses. Currently, there exists no theory that can explain this tendency and future studies should address this important issue. We should also investigate if this correlation can be extended to a metallicity beyond our considered range.

For our study, we have investigated the code dependencies of RSG models, and found that the Hayashi lines predicted from different numerical methods including MESA, BEC, and TWIN codes agree remarkably well, and therefore our calibrated mixing length values may be adopted in other stellar evolution codes that solve the same set of stellar structure equations as in these codes (See Section 3). However, the models by the Geneva group give significantly higher RSG temperatures for a given mixing length parameter, which calls for a future investigation on the impact of numerical schemes employed in different codes.

The final structures of RSGs given by our calibrated mixing length can provide useful predictions on the properties of SN IIP supernova progenitors (Section 5). In particular, the final radii are expected to be about $400 R_{\odot} - 800 R_{\odot}$ for the initial mass range of $10 M_{\odot} \lesssim M_{\text{init}} \lesssim 16 M_{\odot}$ which is typical for SN IIP progenitors (Section 5.2). Our result also implies that the radii of SN IIP progenitors for a given initial mass do not depend on metallicity.

Another important finding in this study (although it is not directly related to the mixing length) is that, for $M_{\text{init}} \gtrsim 15 M_{\odot}$, the hydrogen envelope masses of SN IIP progenitors at SMC and LMC metallicities can be much higher with the Schwarzschild criterion ($M_{\text{H-env}} \simeq 10 - 20$) than with the Ledoux criterion and slow semi-convection ($M_{\text{H-env}} < 10 M_{\odot}$). In the latter case the hydrogen envelope mass does not appear to strongly depend on metallicity (Section 5.1).

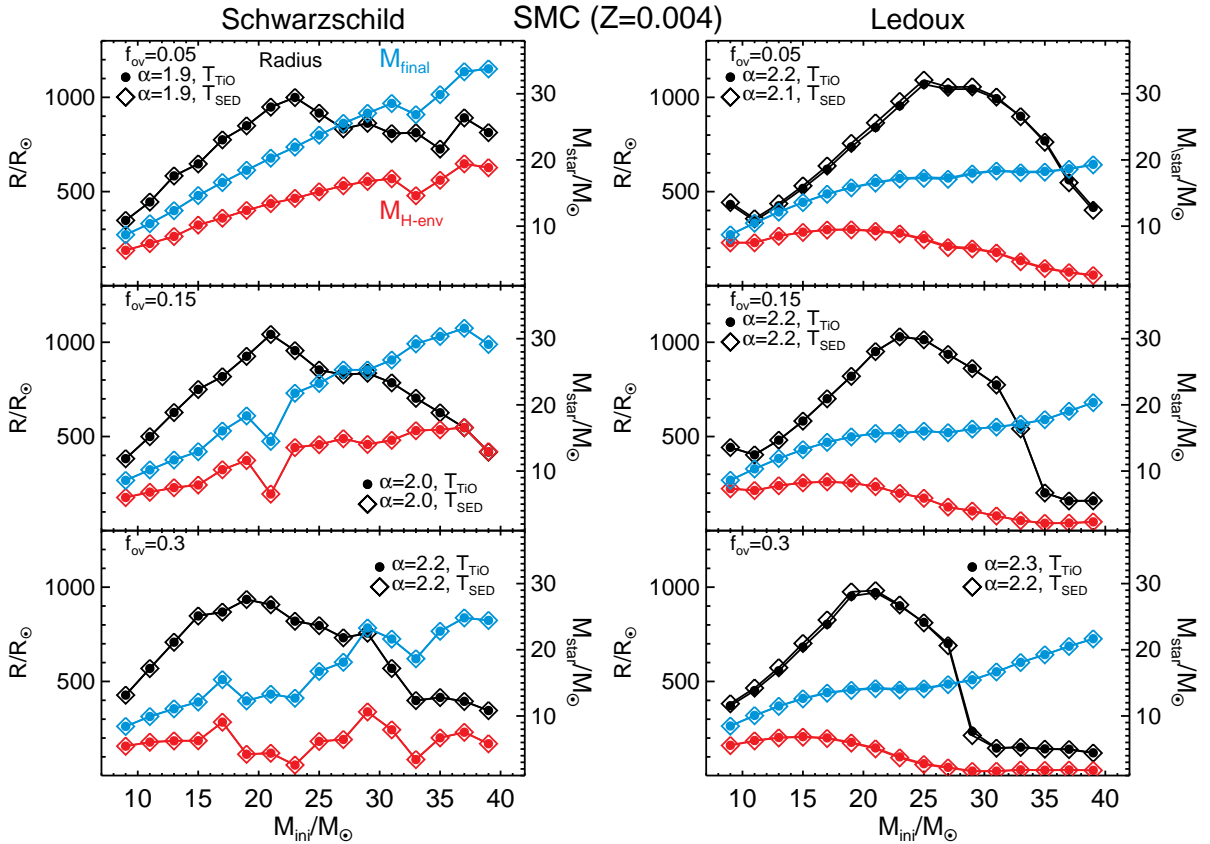


Figure 16. Final radius, final total mass, and final hydrogen-rich envelope mass as a function of the initial mass for the SMC metallicity ($Z=0.004$) predicted from our mixing length calibration with TiO (filled circle) and SED (open diamond) temperatures. The left and right panels present the results with the Schwarzschild and Ledoux models, respectively. The final radii are plotted as black color and their size indicated on the left axis. The final total mass and final hydrogen-rich envelope mass are indicated by blue and red colors, respectively, and their masses are indicated on the right axis. The results of three different overshooting parameters ($f_{\text{ov}} = 0.05, 0.15$, and 0.3) are plotted from the top to bottom panels. In each panel, the calibrated mixing length values by TiO and SED temperatures for the given metallicity and overshooting parameter are indicated by different symbols. Here we excluded models with $M_{\text{H-env}} < 0.5M_{\odot}$.

This could be tested in principle with a sufficiently large sample of SNe IIP from metal poor environments (cf. Anderson et al. 2016).

We are grateful to Georges Meynet, who referred this paper, for many constructive comments that helped us improve the paper. This work was sup-

ported by the Basic Science Research program (NRF-2016R1D1A1A09918398) through the National Research Foundation of Korea (NRF) and by the Korea Astronomy and Space Science Institute under the R&D program (Project No. 3348-20160002) supervised by the Ministry of Science and ICT. SCY acknowledges the support by the Monash Center for Astrophysics via the distinguished visitor program.

APPENDIX

A. APPENDIX MATERIAL

In the figures, we present the final radius, final total mass, and final mass of the hydrogen-rich envelope as a function of the initial mass, which are obtained by interpolating the results of our model sequences at the calibrated mixing length values. Here we excluded models with $M_{\text{H-env}} < 0.5M_{\odot}$.

REFERENCES

Alongi, M., Bertelli, G., Bressan, A., & Chiosi, C. 1991, *A&A*, 244, 95

Anderson, J. P., Gutiérrez, C. P., Dessart, L., et al. 2016, *A&A*, 589, A110

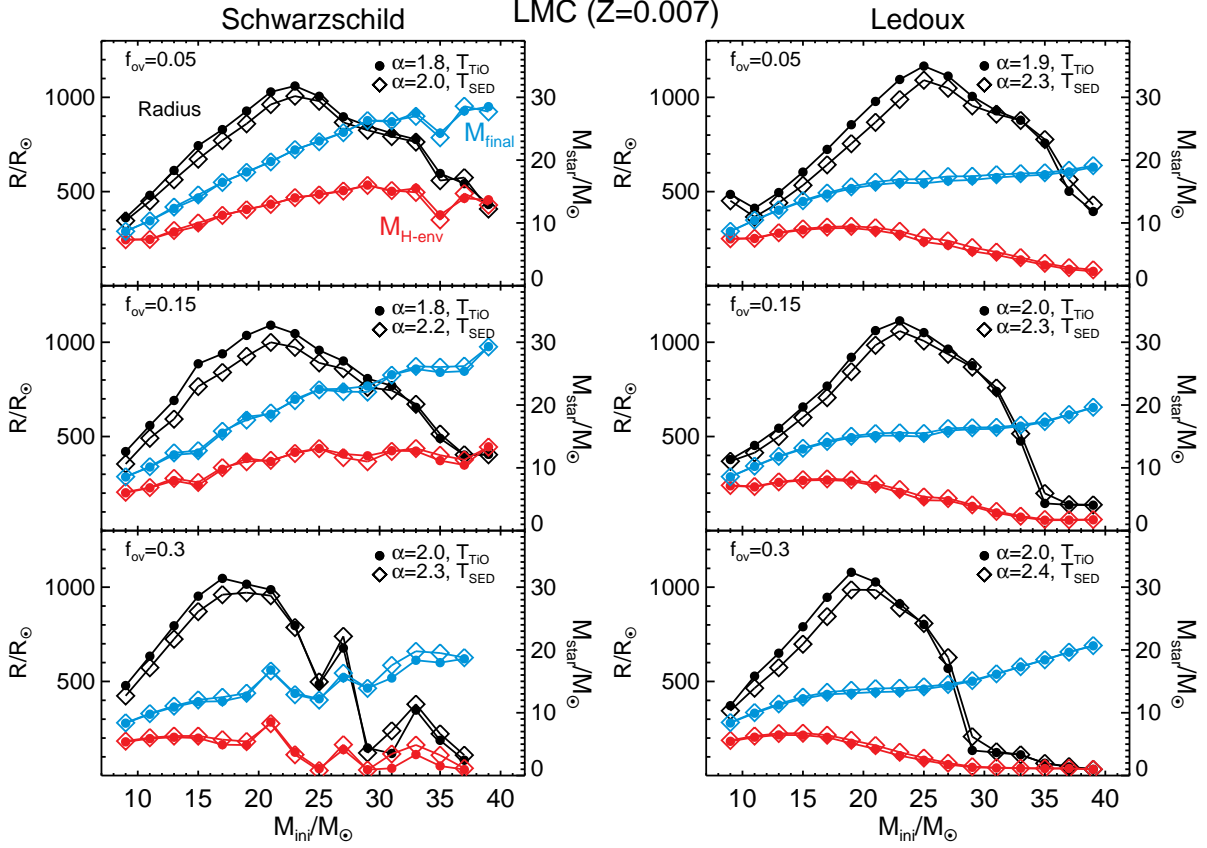


Figure 17. Same with Figure 16 but for LMC metallicity ($Z=0.007$).

Asplund, M., Grevesse, N., & Sauval, A. J. 2005, in *Astronomical Society of the Pacific Conference Series*, Vol. 336, *Cosmic Abundances as Records of Stellar Evolution and Nucleosynthesis*, ed. T. G. Barnes, III & F. N. Bash, 25

Asplund, M., Grevesse, N., Sauval, A. J., & Scott, P. 2009, *ARA&A*, 47, 481

Bono, G., Caputo, F., Cassisi, S., et al. 2000, *ApJ*, 543, 955

Bose, S., Valenti, S., Misra, K., et al. 2015, *MNRAS*, 450, 2373

Brott, I., de Mink, S. E., Cantiello, M., et al. 2011, *A&A*, 530, A115

Chiavassa, A., Freytag, B., Masseron, T., & Plez, B. 2011, *A&A*, 535, A22

Chieffi, A., Straniero, O., & Salaris, M. 1995, *ApJL*, 445, L39

Cunha, K., Hubeny, I., & Lanz, T. 2006, *ApJL*, 647, L143

Davies, B., Kudritzki, R.-P., Gazak, Z., et al. 2015, *ApJ*, 806, 21

Davies, B., Kudritzki, R.-P., Plez, B., et al. 2013, *ApJ*, 767, 3

de Jager, C., Nieuwenhuijzen, H., & van der Hucht, K. A. 1988, *A&AS*, 72, 259

Dessart, L., Hillier, D. J., & Audit, E. 2017, *ArXiv e-prints*, arXiv:1704.01697

Dessart, L., Hillier, D. J., Waldman, R., & Livne, E. 2013, *MNRAS*, 433, 1745

Drout, M. R., Massey, P., Meynet, G., Tokarz, S., & Caldwell, N. 2009, *ApJ*, 703, 441

Eggenberger, P., Meynet, G., & Maeder, A. 2002, *A&A*, 386, 576

Eggleton, P. P. 1971, *MNRAS*, 151, 351

Eggleton, P. P., & Kiseleva-Eggleton, L. 2002, *ApJ*, 575, 461

Ekström, S., Georgy, C., Eggenberger, P., et al. 2012, *A&A*, 537, A146

El Eid, M. F. 1995, *MNRAS*, 275, 983

Eldridge, J. J., Fraser, M., Smartt, S. J., Maund, J. R., & Crockett, R. M. 2013, *MNRAS*, 436, 774

Elias, J. H., Frogel, J. A., & Humphreys, R. M. 1985, *ApJS*, 57, 91

Gabriel, M., Noels, A., Montalbán, J., & Miglio, A. 2014, *A&A*, 569, A63

Garnavich, P. M., Tucker, B. E., Rest, A., et al. 2016, *ApJ*, 820, 23

Gazak, J. Z., Davies, B., Bastian, N., et al. 2014, *ApJ*, 787, 142

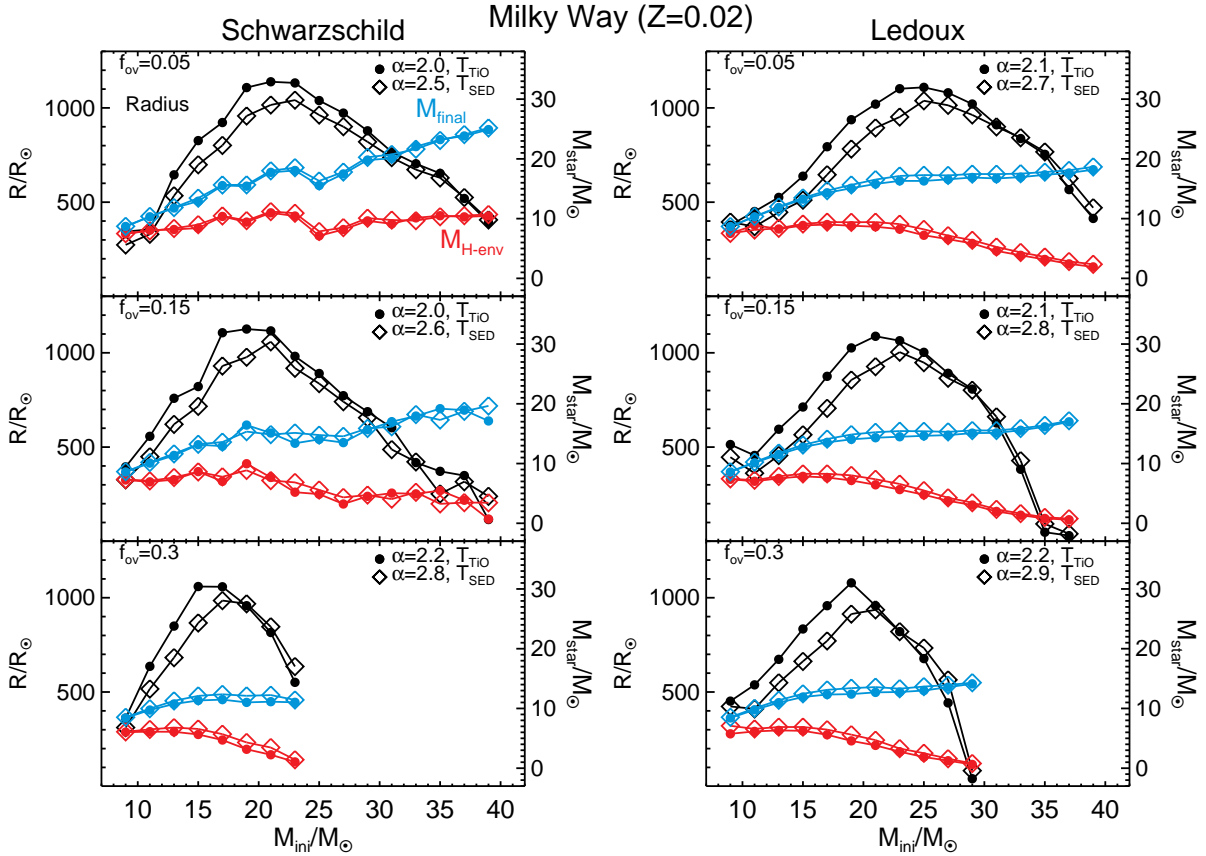


Figure 18. Same with Figure 16 but for solar metallicity ($Z=0.02$).

Gazak, J. Z., Kudritzki, R., Evans, C., et al. 2015, *ApJ*, 805, 182

Georgy, C. 2012, *A&A*, 538, L8

Georgy, C., Ekström, S., Eggenberger, P., et al. 2013, *A&A*, 558, A103

González-Gaitán, S., Tominaga, N., Molina, J., et al. 2015, *MNRAS*, 451, 2212

Gordon, M. S., Humphreys, R. M., & Jones, T. J. 2016, *ApJ*, 825, 50

Grevesse, N., & Sauval, A. J. 1998, *SSRv*, 85, 161

Hayashi, C., & Hoshi, R. 1961, *PASJ*, 13, 442

Heger, A., Langer, N., & Woosley, S. E. 2000, *ApJ*, 528, 368

Izzard, R. G., & Glebbeek, E. 2006, *NewA*, 12, 161

Jones, S., Hirschi, R., Pignatari, M., et al. 2015, *MNRAS*, 447, 3115

Kippenhahn, R., & Weigert, A. 1990, *Stellar Structure and Evolution*, 192

Langer, N. 2012, *ARA&A*, 50, 107

Langer, N., & Maeder, A. 1995, *A&A*, 295, 685

Levesque, E. M., Massey, P., Olsen, K. A. G., et al. 2005, *ApJ*, 628, 973

—. 2006, *ApJ*, 645, 1102

Maeder, A., & Meynet, G. 2000, *ARA&A*, 38, 143

Magic, Z., Weiss, A., & Asplund, M. 2015, *A&A*, 573, A89

Martins, F., & Palacios, A. 2013, *A&A*, 560, A16

Massey, P., & Evans, K. A. 2016, *ApJ*, 826, 224

Massey, P., Silva, D. R., Levesque, E. M., et al. 2009, *ApJ*, 703, 420

Meynet, G., & Maeder, A. 1997, *A&A*, 321, 465

Meynet, G., Chomienne, V., Ekström, S., et al. 2015, *A&A*, 575, A60

Mokiem, M. R., de Koter, A., Evans, C. J., et al. 2006, *A&A*, 456, 1131

Moriya, T. J., Yoon, S.-C., Gräfener, G., & Blinnikov, S. I. 2017, *MNRAS*, 469, L108

Morozova, V., Piro, A. L., Renzo, M., & Ott, C. D. 2016, *ApJ*, 829, 109

Morozova, V., Piro, A. L., & Valenti, S. 2017, *ApJ*, 838, 28

Nakar, E., & Sari, R. 2010, *ApJ*, 725, 904

Patrick, L. R., Evans, C. J., Davies, B., et al. 2015, *ApJ*, 803, 14

Paxton, B., Bildsten, L., Dotter, A., et al. 2011, *ApJS*, 192, 3

Paxton, B., Cantiello, M., Arras, P., et al. 2013, *ApJS*, 208, 4

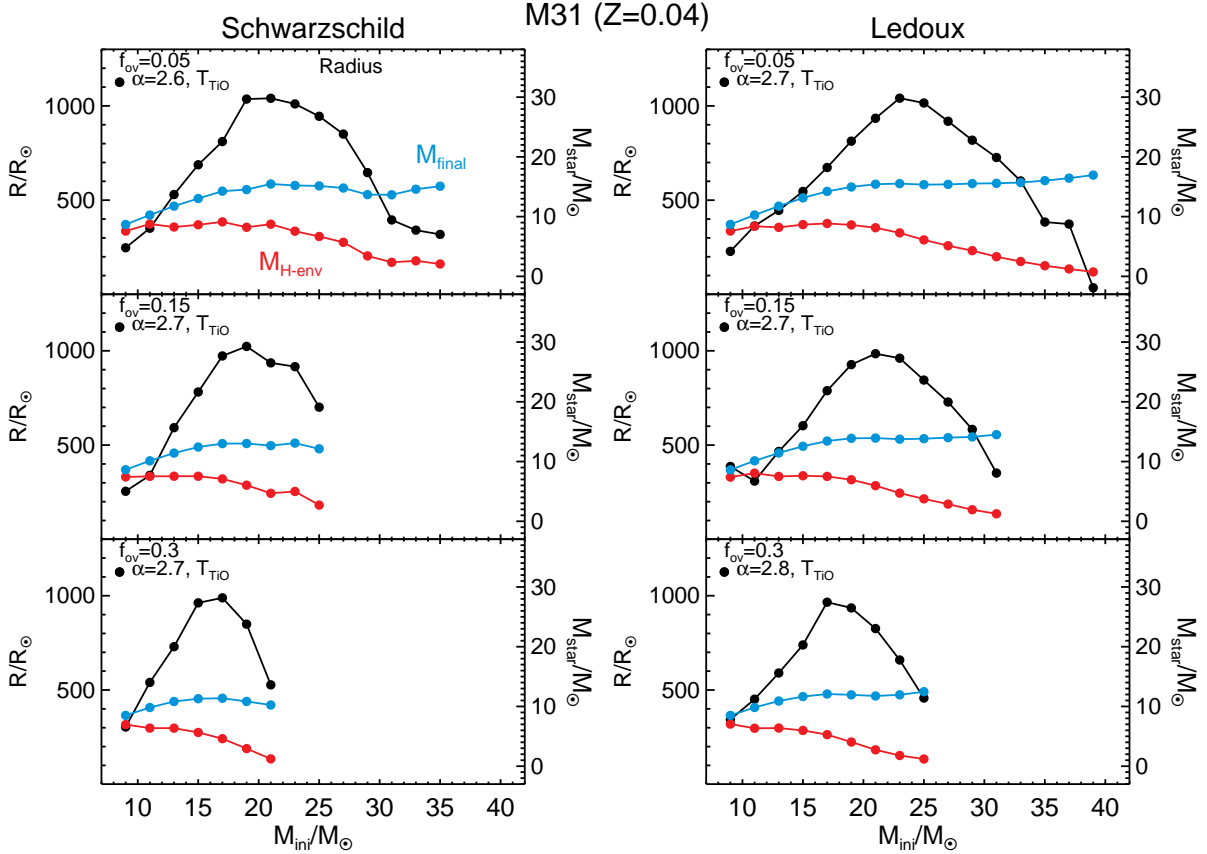


Figure 19. Same with Figure 16 but for M31 metallicity ($Z=0.04$).

- Paxton, B., Marchant, P., Schwab, J., et al. 2015, *ApJS*, 220, 15
- Paxton, B., Schwab, J., Bauer, E. B., et al. 2017, *ArXiv e-prints*, arXiv:1710.08424
- Podsiadlowski, P., Joss, P. C., & Hsu, J. J. L. 1992, *ApJ*, 391, 246
- Rabinak, I., & Waxman, E. 2011, *ApJ*, 728, 63
- Ramírez-Agudelo, O. H., Simón-Díaz, S., Sana, H., et al. 2013, *A&A*, 560, A29
- Sanders, N. E., Caldwell, N., McDowell, J., & Harding, P. 2012, *ApJ*, 758, 133
- Schaller, G., Schaerer, D., Meynet, G., & Maeder, A. 1992, *A&AS*, 96, 269
- Shussman, T., Waldman, R., & Nakar, E. 2016, *ArXiv e-prints*, arXiv:1610.05323
- Simón-Díaz, S., & Herrero, A. 2014, *A&A*, 562, A135
- Smartt, S. J. 2009, *ARA&A*, 47, 63
- . 2015, *PASA*, 32, e016
- Smith, N. 2014, *ARA&A*, 52, 487
- Stothers, R. B., & Chin, C.-W. 1991, *ApJ*, 374, 288
- . 1996, *ApJ*, 469, 166
- Tayar, J., Somers, G., Pinsonneault, M. H., et al. 2017, *ApJ*, 840, 17
- Utrobin, V. P., & Chugai, N. N. 2009, *A&A*, 506, 829
- Valenti, S., Sand, D., Pastorello, A., et al. 2014, *MNRAS*, 438, L101
- van Loon, J. T. 2006, in *Astronomical Society of the Pacific Conference Series*, Vol. 353, *Stellar Evolution at Low Metallicity: Mass Loss, Explosions, Cosmology*, ed. H. J. G. L. M. Lamers, N. Langer, T. Nugis, & K. Annuk, 211
- Vink, J. S., de Koter, A., & Lamers, H. J. G. L. M. 2001, *A&A*, 369, 574
- Yoon, S.-C., & Cantiello, M. 2010, *ApJL*, 717, L62
- Yoon, S.-C., Dessart, L., & Clocchiatti, A. 2017, *ApJ*, 840, 10
- Zaussinger, F., & Spruit, H. C. 2013, *A&A*, 554, A119